Chemistry–A European Journal

Supporting Information

Tunable Linear and Nonlinear Optical Properties from Room Temperature Phosphorescent Cyclic Triimidazole-Pyrene Bio-Probe

Andrea Previtali, Wei He, Alessandra Forni,* Daniele Malpicci, Elena Lucenti, Daniele Marinotto, Lucia Carlucci,* Pierluigi Mercandelli, Marco Aldo Ortenzi, Giancarlo Terraneo, Chiara Botta, Ryan Tsz Kin Kwok, Jacky Wing Yip Lam, Ben Zhong Tang,* and Elena Cariati*

1. Experimental details

1.1 General Information

All reagents were purchased from chemical suppliers and used without further purification unless otherwise stated. Triimidazo[1,2-*a*:1',2'-*c*:1'',2''-*e*][1,3,5]triazine (**TT**)[1] and 3-bromotriimidazo[1,2-*a*:1',2'-*c*:1'',2''-*e*][1,3,5]triazine (**TT1Br**)[2] were prepared according to literature procedures.

^{1}H and ^{13}C NMR spectra were recorded on a Bruker AVANCE-400 instrument (400 MHz). Chemical shifts are reported in parts per million (ppm) and are referenced to the residual solvent peak (DMSO, ^{1}H 2.50 ppm, ^{13}C 40.00 ppm). Coupling constants (*J*) are given in hertz (Hz) and are quoted to the nearest 0.5 Hz. Peak multiplicities are described in the following way: s, singlet; d, doublet; m. multiplet.

Mass spectra were recorded on a Thermo Fisher LCQ Fleet Ion Trap Mass Spectrometer equipped with UltiMate™ 3000 HPLC system.

UV-Visible spectra were collected by a Shimadzu UV3600 spectrophotometer.

Absolute photoluminescence quantum yields were measured using a C11347 (Hamamatsu Photonics K.K). A description of the experimental setup and measurement method can be found in the article of K. Suzuki et al.[3] For any fixed excitation wavelength, the fluorescence quantum yield Φ is given by:

$$\Phi = \frac{\mathrm{PN(Em)}}{\mathrm{PN(Abs)}} = \frac{\int \frac{\lambda}{hc}\left[\mathrm{I_{em}^{sample}}(\lambda) - \mathrm{I_{em}^{reference}}(\lambda)\right] \mathrm{d}\lambda}{\int \frac{\lambda}{hc}\left[\mathrm{I_{ex}^{reference}}(\lambda) - \mathrm{I_{ex}^{sample}}(\lambda)\right] \mathrm{d}\lambda}$$

where PN(Em) is the number of photons emitted from a sample and PN(Abs) is the number of photons absorbed by a sample, λ is the wavelength, h is Planck's constant, c is the velocity of light, $\mathrm{I_{em}^{sample}}(\lambda)$ and $\mathrm{I_{em}^{reference}}(\lambda)$ are the photoluminescence intensities with and without a sample, respectively, $\mathrm{I_{ex}^{sample}}(\lambda)$ and $\mathrm{I_{ex}^{reference}}(\lambda)$ are the integrated intensities of the excitation light with and without a sample, respectively. PN(Em) is calculated in the wavelength interval [λ_i, λ_f], where λ_i is taken 10 nm below the excitation wavelength, while λ_f is the upper end wavelength in the emission spectrum. The error made was estimated at around 5%.

Steady state emission and excitation spectra and photoluminescence lifetimes were obtained using a FLS 980 (Edinburg Instrument Ltd) and a Nanolog (Horiba Scientific) spectrofluorimeter. The steady state measurements were recorded by a 450 W Xenon arc lamp. Photoluminescence lifetime measurements were performed using: Edinburgh Picosecond Pulsed Diode Laser EPL-375, EPL-405, EPLED-300, (Edinburg Instrument Ltd) and microsecond flash Xe-lamp (60W, 0.1÷100 Hz) with data acquisition devices time

correlated single-photon counting (TCSPC) and multi-channel scaling (MCS) methods, respectively. Average lifetimes are obtained as:

$\tau_{av} \equiv \frac{\sum_{n=1}^{m} \alpha_n \tau_n^2}{\sum_{n=1}^{m} \alpha_n \tau_n}$, where m is the multi-exponential decay number of the fit.

Low temperature measurements are performed by immersion of the sample in a N_2 quartz dewar or with a variable temperature liquid nitrogen cryostat Oxford DN1704.

Films of **TTPyr** dispersed in polymethylmethacrylate (PMMA) were prepared by spin coating (2000 rpm, 60s) few drops of a DCM solution (**TTPyr**/PMMA = 0.5 and 5 wt%; PMMA = 10 wt% with respect to the solvent) on a quartz substrate. Amorphous films have been prepared by melting at 300°C powders of **TTPyr** (5 mg) on a quartz substrate and rapidly quenching the melt with liquid nitrogen. Cast films were prepared by casting few drops of a dichloromethane solution ($6x10^{-3}$ M) of **TTPyr** on a quartz substrate, followed by evaporation to dryness in air at room temperature.

Second Harmonic Generation (SHG) of powdered samples was measured by the Kurtz and Perry method[4]. The non-resonant 1064 nm wavelength of a Nd:YAG pulsed laser beam was directed on capillaries containing the samples. The scattered radiation was collected by an elliptical mirror, filtered to select only the second-order contribution at 532 nm, and recollected with a Hamamatsu R 5108 photomultiplier tube. The SHG efficiency was evaluated by taking as reference the SHG signal of urea powders.

1.2 Thermal analysis

DSC analyses were conducted using a Mettler Toledo DSC1 (Mettler Toledo, Columbus, OH, USA), on a sample weighing about 3 mg. Melting and crystallization temperatures were measured heating from 25°C to 320°C at 10°C/min under N_2 flux. TGA was performed using a TGA 4000 Perkin Elmer instrument. The analysis was conducted under air atmosphere on a sample weighing about 10 mg, using a program that provides a single heating cycle from 30 to 500 °C at 20 °C/min.

1.3 VT-XRPD

In-situ variable temperature powder XRD data were collected on a Bruker D8 Advance diffractometer using Cu Kα1 radiation (λ = 1.5406 Å) and equipped with Lynx Eye detector. The measurements were carried out in Bragg-Brentano geometry with a step size of 0.031° and exposure time of 1.0 s in a 2θ range of 5−30°. The scanned temperature range was from 25° C to 310°C.

1.4 Crystal Structure Analysis

Single-crystal X-ray diffraction data for the three phases **TTPyr(Et)**, **TTPyr(RT)** and **TTPyr(HT)** were collected at room temperature on a Bruker APEX II CCD area detector diffractometer, using graphite-monochromated Mo *K*α radiation (λ = 0.71073 Å). A full sphere of reciprocal space was scanned by 0.5° ω steps, collecting 2160 frames in six different regions of the reciprocal space. After integration, an empirical absorption correction was made on the basis of the symmetry-equivalent reflection intensities measured.[5]

The structures were solved by direct methods (SIR 2014[6]) and subsequent Fourier synthesis; they were refined by full-matrix least-squares on F^2 (SHELX 2014[7]) using all reflections. Weights were assigned to individual observations according to the formula $w = 1/[\sigma^2(F_o^2) + (aP)^2 + bP]$, where $P = (F_o^2 + 2F_c^2)/3$; a and b were chosen to give a flat analysis of variance in terms of F_o^2. Anisotropic parameters were assigned to all non-hydrogen atoms. All the hydrogen atoms were clearly visible in difference-Fourier maps (except those of the disordered ethanol molecule in **TTPyr(Et)**); however, they were eventually placed in idealized position and refined riding on their parent atom with an isotropic displacement parameter 1.2 (or 1.5) times that of the pertinent parent atom.

The final difference electron density map showed no features of chemical significance, with the largest peaks lying close to the center of bonds.

In the structure of **TTPyr(Et)** the ethanol molecule is disordered over the Wyckoff position 4*e* (site symmetry 2). The molecule was refined anisotropically applying soft restraints on 1,2 and 1,3 atomic distances. The ethanol content is in agreement with the results of elemental and thermogravimetric analyses.

model was found and the coordinates are reported in the supplementary materials

Crystal data, data collection and refinement details of the structural analyses are summarized in Table S1, while a selection of geometric parameters for the three phases are collected in Tables S2–S4. CCDC 2079770–2079772 contain the supplementary crystallographic data for **TTPyr(Et)**, **TTPyr(RT)** and **TTPyr(HT)**. These data can be obtained free of charge from the Cambridge Crystallographic Data Centre http://www.ccdc.cam.ac.uk/conts/retrieving.html.

Despite many attempts, performed both at room and low temperature, diffraction data collected for the phase **TTPyr(Me)** were always of limited quality, leading to a model that could not be fully refined. Tentative coordinates are reported in Table S5.

1.5 Computational details

DFT and TDDFT calculations on **TTPyr** were performed with Gaussian 16 program (Revision A.03) [8] using the 6-311++G(d,p) basis set. The geometries of **TTPyr** and its dimers have been optimized starting from the experimental structures as derived from X-ray studies. Based on previous theoretical results as obtained on the parent cyclic triimidazole and its pyridine- and cloro-, bromo- and iododerivatives, the ωB97X [9] functional was used owing to its ability in correctly treating at the same time not only ground and excited states properties, but also intermolecular interactions.

*1.6 Synthesis of 3-(pyren-1-yl)triimidazo[1,2-a:1',2'-c:1'',2''-e][1,3,5]triazine (**TT-Pyr**)*

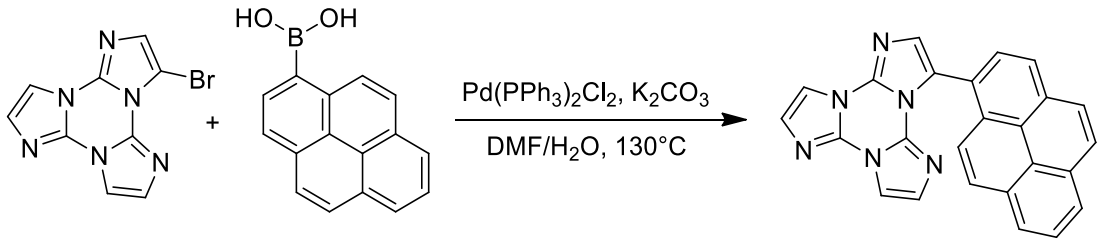

TT-Pyr

TTPyr is prepared by Suzuki coupling between **TT1Br** and pyrene-1-boronic acid. In a typical reaction, **TT1Br** (200 mg; 0.72 mmol), pyren-1-ylboronic acid (246 mg, 1.01 mmol), potassium carbonate (400 mg, 2.88 mmol), $Pd(PPh_3)_2Cl_2$ (25 mg, 0.03 mmol), water (2mL) and DMF (10 mL) are transferred inside a 100 mL Schlenk flask equipped with a magnetic stirrer. The system is heated under static nitrogen atmosphere at 130 °C for 12 h. The reaction is then cooled to room temperature, precipitated with water (100 mL) and filtered on a buchner. The solid crude reaction mixture is further purified by automated flash chromatography on SiO_2 with DCM/MeOH as eluents to give the product as a pale yellow solid (258 mg; Yield 90%; R_f,=0.7 in DCM/MeOH =95/5). Long needled shaped crystals suitable for single crystal X-ray diffraction analysis are obtained by slow evaporation at room temperature of DCM/hexane (8/2) or DCM/EtOH (8/2) solutions, to give **TTPyr(Hex)** and **TTPyr(Et)**, respectively.

NMR data (9.4 T, DMSO-d_6, 298 K, δ, ppm): ^{1}H NMR 8.38 (1H, d, *J* = 7.8 Hz), 8.37 (1H, d, *J* = 7.5 Hz), 8.29 (3H, m), 8.18 (1H, d, *J* = 7.8 Hz), 8.10 (4H, m), 7.86 (1H, d, *J* = 1.5 Hz), 7.46 (1H, s), 7.35 (1H, d, *J* = 1.6 Hz), 6.81 (1H, d, *J* = 1.5 Hz); **^{13}C NMR** 137.02, 136.32, 131.96, 131.35, 131.25, 130.90, 130.20 (*C*H), 129.02 (*C*H), 128.95 (*C*H), 128.62 (*C*H), 128.54 (*C*H), 128.16 (*C*H), 127.84 (*C*H), 126.97 (*C*H), 126.25 (*C*H), 126.11 (*C*H), 125.98 (*C*H), 125.65, 124.70 (*C*H), 124.16, 124.01, 112.28 (*C*H), 111.42 (*C*H).

LC-MS analysis: Gradient 5/95 CH_3CN/H_2O to 100/0 CH_3CN/H_2O in 60 min m/z = 399; r.t= 45.59

MS (ESI-positive ion mode): *m/z*: 399 $[M+H]^+$. r.t= 45.59 min. Gradient 5/95 CH_3CN/H_2O to 100/0 CH_3CN/H_2O in 60 min.

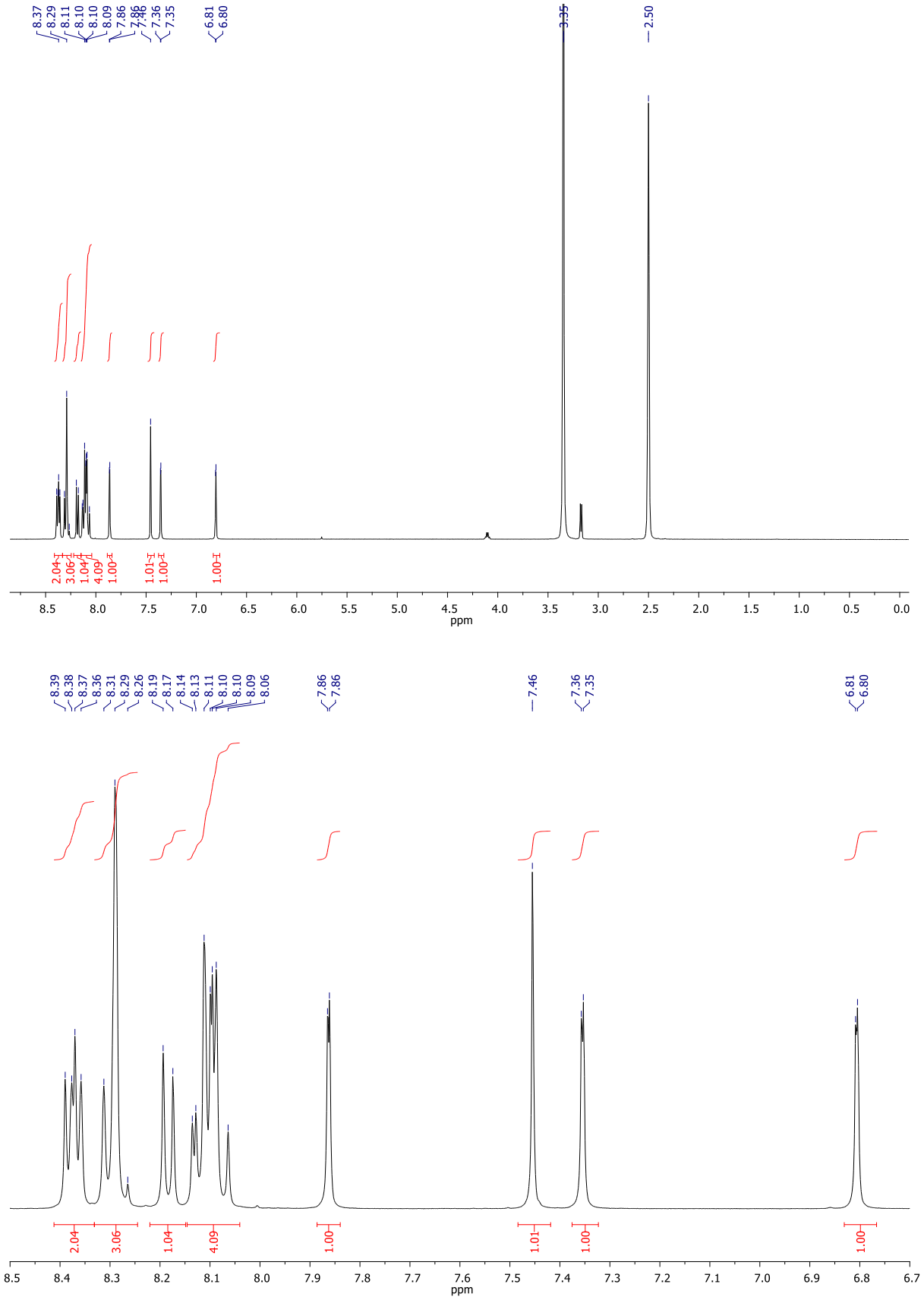

Figure S1. ^{1}H NMR spectrum and expanded region of **TTPyr** (400 MHz, DMSO-d_6)

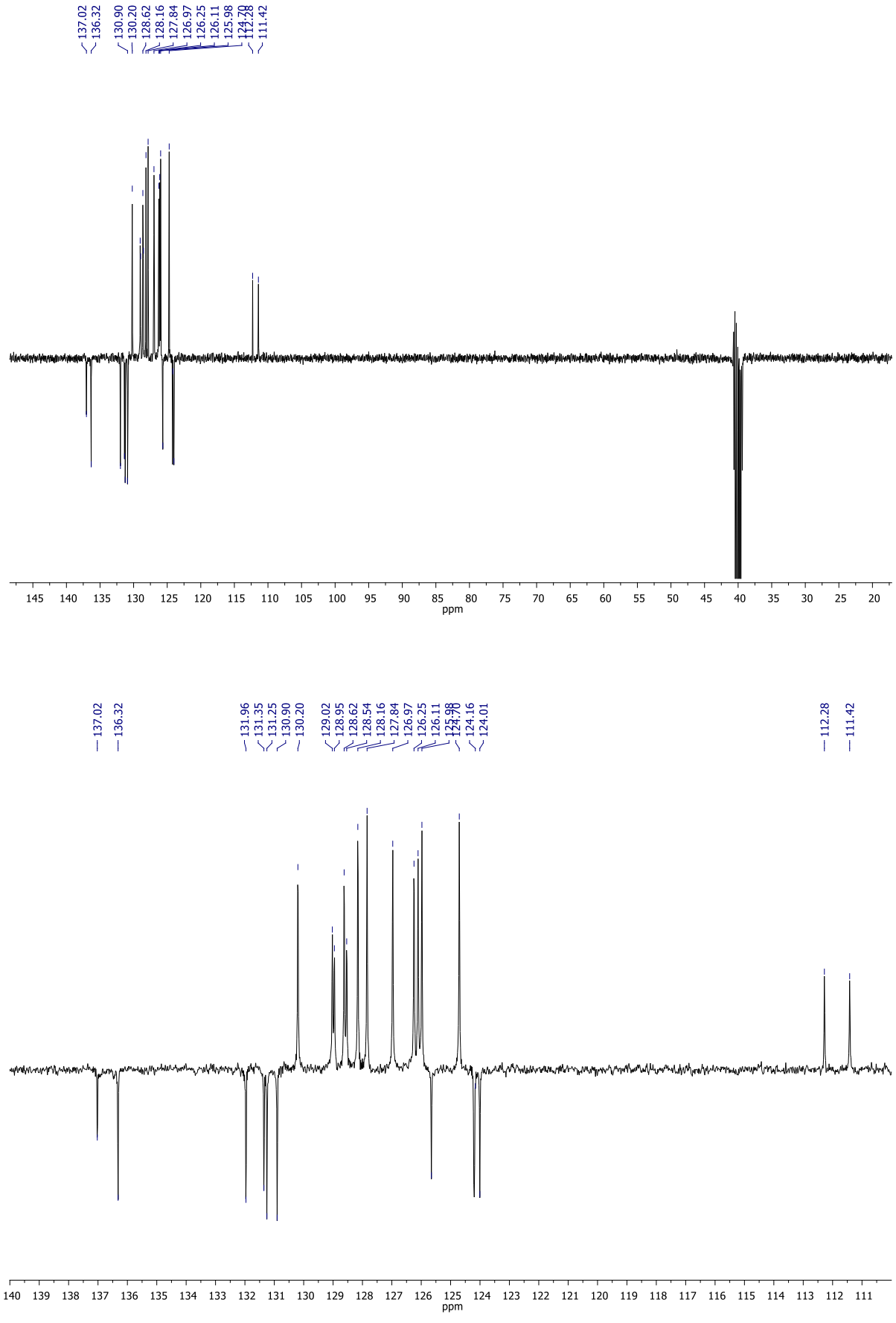

Figure S2. ^{13}C NMR spectrum and expanded region of **TTPyr** (100 MHz, DMSO-d_6)

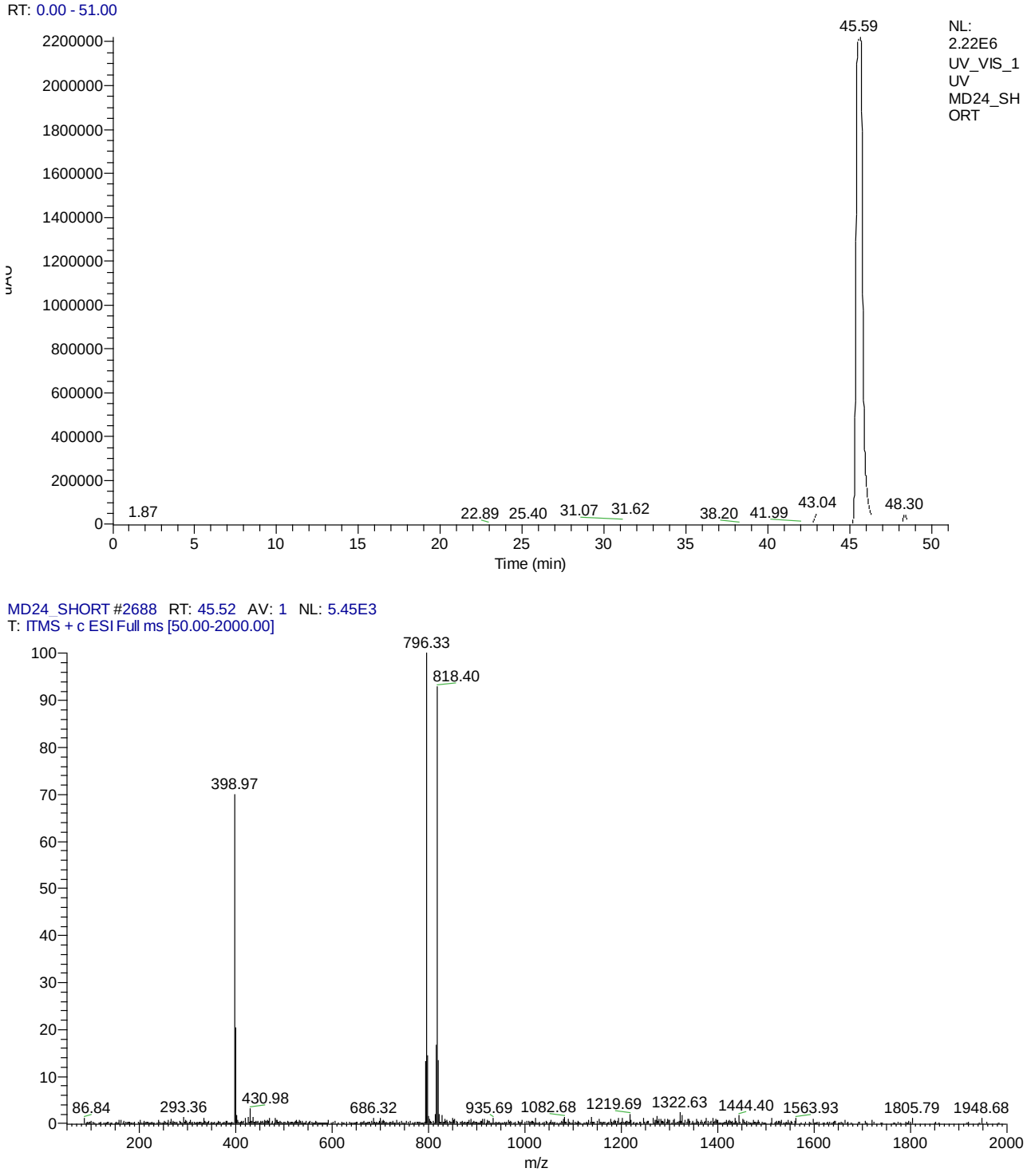

Figure S3. LC-MS profile of **TTPyr**

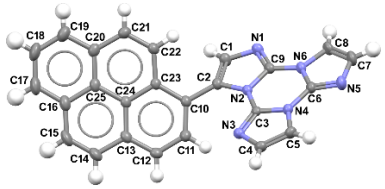

Figure S4. A single molecule of TTPyr of the **TTPyr(RT)** phase with the labelling scheme. The same labelling scheme is used for **TTPyr(Et)** and **TTPyr(HT)**.

Table S1 Crystal data, data collection and refinement details for **TTPyr(Et)**, **TTPyr(RT)** and **TTPyr(HT)**

	TTPyr(Et)	**TTPyr(RT)**	**TTPyr(HT)**
Crystal data			
Chemical formula	$C_{25}H_{14}N_6 \cdot ½C_2H_6O$ = $C_{26}H_{17}N_6O_{0.5}$	$C_{25}H_{14}N_6$	$C_{25}H_{14}N_6$
M_r	421.45	398.42	398.42
Crystal system	monoclinic	monoclinic	orthorhombic
Space group	C2/c (No. 15)	$P2_1/c$ (No. 14)	$Pna2_1$ (No. 33)
Temperature [K]	295(2)	295(2)	295(2)
a [Å]	34.733(2)	15.9433(17)	7.7788(5)
b [Å]	7.6847(5)	7.7728(8)	29.2508(18)
c [Å]	16.1652(11)	15.9868(17)	8.1316(5)
α [°]	90	90	90
β [°]	115.630(2)	113.590(2)	90
γ [°]	90	90	90
V [$Å^3$]	3890.1(5)	1815.6(3)	1850.2(2)
Z	8	4	4
μ(MoKα) [mm^{-1}]	0.091	0.091	0.089
Crystal size [mm]	0.750 × 0.260 × 0.025	0.585 × 0.135 × 0.045	0.415 × 0.075 × 0.070
Data collection			
T_{min}, T_{max}	0.951, 0.998	0.932, 0.996	0.925, 0.994
No. of measured reflections	38820	34417	35258
No. of independent reflections	4833	4519	4567
No. of observed reflections [I > 2σ(I)]	2982	3375	3584
R_{int}	0.0268	0.0195	0.0245
$R_σ$	0.0443	0.0319	0.0394
$(\sin θ/λ)_{max}$ [$Å^{-1}$]	0.667	0.667	0.666
Refinement			
$R[F^2 > 2σ(F^2)]$	0.0496	0.0499	0.0785
$wR(F^2)$	0.1475	0.1340	0.1068
S	1.015	1.017	1.210
No. of reflections	4833	4519	4567
No. of parameters	307	280	280
No. of restraints	3	0	1
$Δρ_{max}$, $Δρ_{min}$ (e $Å^{-3}$)	0.517, –0.253	0.216, –0.219	0.136, –0.216

Table S2 Bond distances [Å] and angles [°] for **TTPyr(Et)**

C1–C2	1.357(2)	C2–C1–N1	113.77(16)	C24–C23–C10	118.77(15)
C1–N1	1.374(2)	C1–C2–N2	103.56(15)	C24–C23–C22	117.47(15)
C2–N2	1.412(2)	C1–C2–C10	129.30(16)	C10–C23–C22	123.75(16)
C2–C10	1.470(2)	N2–C2–C10	126.97(14)	C13–C24–C23	120.72(15)
C3–N3	1.295(2)	N3–C3–N4	112.66(14)	C13–C24–C25	119.07(15)
C3–N4	1.369(2)	N3–C3–N2	130.14(15)	C23–C24–C25	120.20(15)
C3–N2	1.397(2)	N4–C3–N2	117.19(14)	C20–C25–C16	119.27(17)
C4–C5	1.335(3)	C5–C4–N3	112.05(16)	C20–C25–C24	120.43(16)
C4–N3	1.384(2)	C4–C5–N4	105.15(16)	C16–C25–C24	120.30(16)
C5–N4	1.385(2)	N5–C6–N6	113.79(17)	C9–N1–C1	103.09(14)
C6–N5	1.298(2)	N5–C6–N4	129.34(18)	C9–N2–C3	121.20(14)
C6–N6	1.360(2)	N6–C6–N4	116.87(15)	C9–N2–C2	105.10(13)
C6–N4	1.382(2)	C8–C7–N5	113.10(18)	C3–N2–C2	133.64(14)
C7–C8	1.339(3)	C7–C8–N6	104.27(18)	C3–N3–C4	104.07(14)
C7–N5	1.385(3)	N1–C9–N2	114.46(15)	C3–N4–C6	123.57(15)
C8–N6	1.392(2)	N1–C9–N6	127.27(16)	C3–N4–C5	106.06(14)
C9–N1	1.293(2)	N2–C9–N6	118.24(15)	C6–N4–C5	130.37(15)
C9–N2	1.376(2)	C11–C10–C23	118.83(15)	C6–N5–C7	102.79(17)
C9–N6	1.382(2)	C11–C10–C2	120.42(15)	C6–N6–C9	122.91(15)
C10–C11	1.396(2)	C23–C10–C2	120.55(14)	C6–N6–C8	106.04(16)
C10–C23	1.422(2)	C12–C11–C10	121.92(17)	C9–N6–C8	131.01(16)
C11–C12	1.373(2)	C11–C12–C13	121.27(16)		
C12–C13	1.390(3)	C12–C13–C24	118.44(16)		
C13–C24	1.421(2)	C12–C13–C14	122.67(16)		
C13–C14	1.433(3)	C24–C13–C14	118.89(17)		
C14–C15	1.337(3)	C15–C14–C13	121.55(18)		
C15–C16	1.424(3)	C14–C15–C16	121.87(18)		
C16–C17	1.394(3)	C17–C16–C15	123.09(19)		
C16–C25	1.424(3)	C17–C16–C25	118.61(19)		
C17–C18	1.379(3)	C15–C16–C25	118.30(18)		
C18–C19	1.374(3)	C18–C17–C16	121.2(2)		
C19–C20	1.391(3)	C19–C18–C17	120.6(2)		
C20–C25	1.420(2)	C18–C19–C20	120.7(2)		
C20–C21	1.429(2)	C19–C20–C25	119.50(18)		
C21–C22	1.345(2)	C19–C20–C21	122.74(17)		
C22–C23	1.435(2)	C25–C20–C21	117.76(16)		
C23–C24	1.422(2)	C22–C21–C20	121.88(16)		
C24–C25	1.429(2)	C21–C22–C23	122.18(16)		

Table S3 Bond distances [Å] and angles [°] for **TTPyr(RT)**

C1–C2	1.356(2)	C2–C1–N1	113.52(13)	C24–C23–C10	118.86(13)
C1–N1	1.376(2)	C1–C2–N2	103.82(13)	C24–C23–C22	123.88(13)
C2–N2	1.4114(18)	C1–C2–C10	129.71(14)	C10–C23–C22	117.25(13)
C2–C10	1.476(2)	N2–C2–C10	126.39(12)	C13–C24–C23	120.30(13)
C3–N3	1.2949(18)	N3–C3–N4	112.94(13)	C13–C24–C25	119.49(13)
C3–N4	1.3708(18)	N3–C3–N2	129.86(13)	C23–C24–C25	120.22(13)
C3–N2	1.3966(17)	N4–C3–N2	117.20(12)	C20–C25–C16	119.42(15)

C4–C5	1.339(2)	C5–C4–N3	112.08(13)	C20–C25–C24	120.42(14)
C4–N3	1.3837(19)	C4–C5–N4	105.21(13)	C16–C25–C24	120.16(15)
C5–N4	1.3824(19)	N5–C6–N6	114.17(14)	C9–N1–C1	103.15(12)
C6–N5	1.2956(19)	N5–C6–N4	129.41(15)	C9–N2–C3	121.27(12)
C6–N6	1.361(2)	N6–C6–N4	116.42(13)	C9–N2–C2	104.84(11)
C6–N4	1.3828(19)	C8–C7–N5	112.81(15)	C3–N2–C2	133.82(12)
C7–C8	1.341(3)	C7–C8–N6	104.72(15)	C3–N3–C4	103.86(12)
C7–N5	1.384(2)	N1–C9–N2	114.66(13)	C3–N4–C6	105.90(12)
C8–N6	1.3888(18)	N1–C9–N6	127.36(14)	C3–N4–C5	123.75(13)
C9–N1	1.2888(19)	N2–C9–N6	117.96(13)	C6–N4–C5	130.35(13)
C9–N2	1.3779(17)	C11–C10–C23	119.18(13)	C6–N5–C7	102.76(14)
C9–N6	1.3826(19)	C11–C10–C2	119.86(13)	C6–N6–C9	123.38(12)
C10–C11	1.394(2)	C23–C10–C2	120.83(13)	C6–N6–C8	105.55(13)
C10–C23	1.416(2)	C12–C11–C10	121.78(14)	C9–N6–C8	131.06(14)
C11–C12	1.377(2)	C11–C12–C13	120.92(14)		
C12–C13	1.388(2)	C12–C13–C24	118.96(14)		
C13–C24	1.420(2)	C12–C13–C14	122.38(15)		
C13–C14	1.438(2)	C24–C13–C14	118.66(15)		
C14–C15	1.340(3)	C15–C14–C13	121.28(17)		
C15–C16	1.423(3)	C14–C15–C16	122.03(16)		
C16–C17	1.402(3)	C17–C16–C15	123.07(18)		
C16–C25	1.423(2)	C17–C16–C25	118.54(19)		
C17–C18	1.378(3)	C15–C16–C25	118.38(16)		
C18–C19	1.372(3)	C18–C17–C16	121.12(19)		
C19–C20	1.399(2)	C19–C18–C17	120.89(18)		
C20–C25	1.420(2)	C18–C19–C20	120.55(19)		
C20–C21	1.424(2)	C19–C20–C25	119.46(16)		
C21–C22	1.346(2)	C19–C20–C21	122.54(17)		
C22–C23	1.436(2)	C25–C20–C21	118.00(14)		
C23–C24	1.4250(19)	C22–C21–C20	121.75(15)		
C24–C25	1.427(2)	C21–C22–C23	122.33(14)		

Table S4 Bond distances [Å] and angles [°] for **TTPyr(HT)**

C1–C2	1.357(4)	C2–C1–N1	112.8(3)	C24–C23–C10	118.5(3)
C1–N1	1.387(4)	C1–C2–N2	104.4(2)	C24–C23–C22	123.7(2)
C2–N2	1.406(4)	C1–C2–C10	129.5(3)	C10–C23–C22	117.8(3)
C2–C10	1.475(4)	N2–C2–C10	126.1(2)	C13–C24–C23	119.8(2)
C3–N3	1.294(4)	N3–C3–N4	113.4(3)	C13–C24–C25	120.3(3)
C3–N4	1.374(4)	N3–C3–N2	129.5(3)	C23–C24–C25	119.9(3)
C3–N2	1.393(4)	N4–C3–N2	117.1(2)	C20–C25–C16	120.5(2)
C4–C5	1.337(5)	C5–C4–N3	112.5(3)	C20–C25–C24	119.6(3)
C4–N3	1.390(5)	C4–C5–N4	105.1(3)	C16–C25–C24	119.8(3)

C5–N4	1.386(4)	N5–C6–N6	113.8(3)	C9–N1–C1	103.3(2)
C6–N5	1.293(4)	N5–C6–N4	129.6(3)	C9–N2–C3	121.5(2)
C6–N6	1.362(4)	N6–C6–N4	116.6(3)	C9–N2–C2	105.2(2)
C6–N4	1.386(4)	C8–C7–N5	112.4(3)	C3–N2–C2	132.8(2)
C7–C8	1.339(6)	C7–C8–N6	105.0(3)	C3–N3–C4	103.3(3)
C7–N5	1.384(5)	N1–C9–N2	114.3(3)	C3–N4–C6	123.2(3)
C8–N6	1.383(4)	N1–C9–N6	128.1(2)	C3–N4–C5	105.7(2)
C9–N1	1.296(4)	N2–C9–N6	117.5(3)	C6–N4–C5	130.8(3)
C9–N2	1.376(3)	C11–C10–C23	120.1(2)	C6–N5–C7	103.1(3)
C9–N6	1.381(4)	C11–C10–C2	116.6(3)	C6–N6–C9	123.5(2)
C10–C11	1.391(4)	C23–C10–C2	123.2(3)	C6–N6–C8	105.7(3)
C10–C23	1.408(4)	C12–C11–C10	121.0(3)	C9–N6–C8	130.9(3)
C11–C12	1.378(4)	C11–C12–C13	120.9(3)		
C12–C13	1.391(4)	C12–C13–C24	119.0(2)		
C13–C24	1.416(4)	C12–C13–C14	122.2(3)		
C13–C14	1.438(4)	C24–C13–C14	118.8(3)		
C14–C15	1.337(5)	C15–C14–C13	121.4(3)		
C15–C16	1.429(5)	C14–C15–C16	121.6(3)		
C16–C17	1.387(5)	C17–C16–C15	122.9(3)		
C16–C25	1.430(4)	C17–C16–C25	118.6(3)		
C17–C18	1.373(6)	C15–C16–C25	118.6(3)		
C18–C19	1.384(5)	C18–C17–C16	121.4(3)		
C19–C20	1.397(4)	C19–C18–C17	120.9(3)		
C20–C25	1.415(4)	C18–C19–C20	120.3(4)		
C20–C21	1.431(4)	C19–C20–C25	119.3(3)		
C21–C22	1.341(4)	C19–C20–C21	122.9(3)		
C22–C23	1.433(4)	C25–C20–C21	117.8(3)		
C23–C24	1.423(3)	C22–C21–C20	122.0(3)		
C24–C25	1.422(4)	C21–C22–C23	121.6(3)		

Table S5 Tentative fractional coordinates for **TTPyr(Me)**

	x/a	y/b	z/c		x/a	y/b	z/c
C1	0.9097	0.2652	0.3159	H10	1.4470	0.0731	0.5371
H1	0.9393	0.3054	0.3709	C18	1.3632	–0.0144	0.5915
C2	0.9487	0.2012	0.2591	H11	1.4029	–0.0477	0.6433
C3	0.8743	0.0874	0.1056	C19	1.2794	–0.0395	0.5801
C4	0.8885	–0.0215	–0.0081	H12	1.2624	–0.0938	0.6231
H2	0.9142	–0.0658	–0.0469	C20	1.2188	0.0156	0.5040
C5	0.8069	–0.0068	–0.0255	C21	1.1314	–0.0027	0.4890
H3	0.7655	–0.0379	–0.0765	H13	1.1130	–0.0574	0.5310

C6	0.7219	0.1043	0.0670	C22	1.0733	0.0552	0.4169
C7	0.5995	0.1439	0.0750	H14	1.0163	0.0448	0.4118
H4	0.5409	0.1451	0.0598	C23	1.0970	0.1326	0.3476
C8	0.6503	0.1974	0.1523	C24	1.1844	0.1460	0.3592
H5	0.6349	0.2420	0.1984	C25	1.2455	0.0931	0.4374
C9	0.8084	0.2005	0.2062	N1	0.8233	0.2646	0.2841
C10	1.0384	0.1918	0.2692	N2	0.8795	0.1596	0.1857
C11	1.0692	0.2530	0.2035	N3	0.9329	0.0360	0.0744
H6	1.0309	0.2860	0.1508	N4	0.7949	0.0651	0.0483
C12	1.1532	0.2656	0.2145	N5	0.6432	0.0868	0.0204
H7	1.1708	0.3081	0.1694	N6	0.7311	0.1709	0.1475
C13	1.2139	0.2167	0.2917	C26	0.5568	–0.0640	–0.1943
C14	1.3020	0.2339	0.3068	H15	0.5357	–0.0762	–0.2561
H8	1.3213	0.2792	0.2633	H16	0.5126	–0.0907	–0.1699
C15	1.3580	0.1869	0.3816	H17	0.6033	–0.1423	–0.1714
H9	1.4153	0.2028	0.3892	O1	0.5842	0.1069	–0.1732
C16	1.3329	0.1125	0.4506	H18	0.6022	0.1174	–0.1204
C17	1.3895	0.0588	0.5281				

Space group $P2_1/c$ (No. 14). Cell parameters at RT: a = 16.650 Å; b = 7.693 Å; c = 16.245 Å; β = 108.09°.

Thermal Analysis

The TGA trace (Figure S5 top) shows a first weight loss of about 5.6% in the temperature range 145–165°C and a second weight loss in the range 300–410°C corresponding to the complete decomposition of the material with no residue remaining. The first weight loss corresponds to the ethanol departure (computed weight loss 5.46%). The observation that the sample starts to lose weight only at temperature higher than 170°C (b.p. of ethanol 79°C), explains the much higher stability of the ethanol solvate crystals with respect to that of the methanol containing phase.

The DSC analysis performed on **TTPyr(Et)** under nitrogen is shown in Figure S5 middle and bottom. As expected, an endothermic transition corresponding to the ethanol loss is visible between 159 and 173°C (peak at 166°C). A second endothermic transition between 230 and 235°C (peak at 233°C), immediately followed by an exothermic transition between 235 and 251°C (peak at 241°C), corresponds to the melting of the desolvate phase **TTPyr(RT)** and its crystallization to the **TTPyr(HT)** crystal phase. The melting of this last phase is observed between 290 and 294°C (peak at 291°C). Heating/cooling cycles in DSC evidence that the transformation of **TTPyr(RT)** in **TTPyr(HT)** is irreversible, as it is also the desolvation process of **TTPyr(Et)**. In fact, the exposure to ethanol vapor for one night of desolvated samples does not recover the ethanol solvate as confirmed by XRPD monitoring.

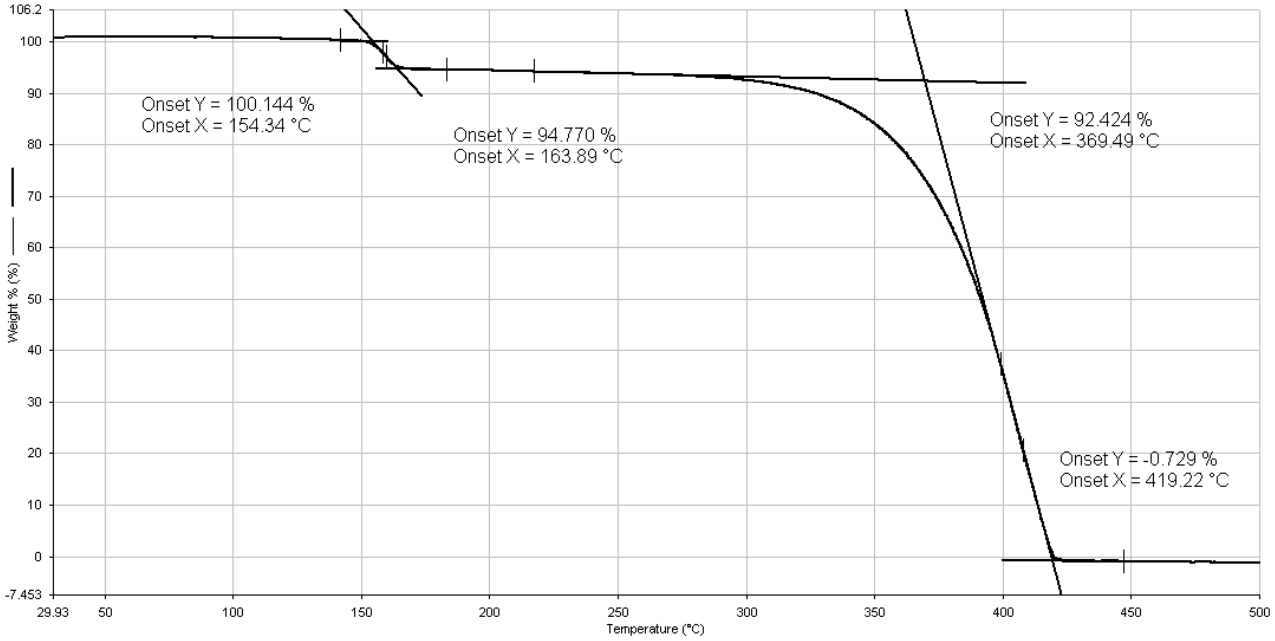
Onset Y = 100.144 %
Onset X = 154.34 °C
Onset Y = 94.770 %
Onset X = 163.89 °C
Onset Y = 92.424 %
Onset X = 369.49 °C
Onset Y = -0.729 %
Onset X = 419.22 °C
Weight % (%)
Temperature (°C)

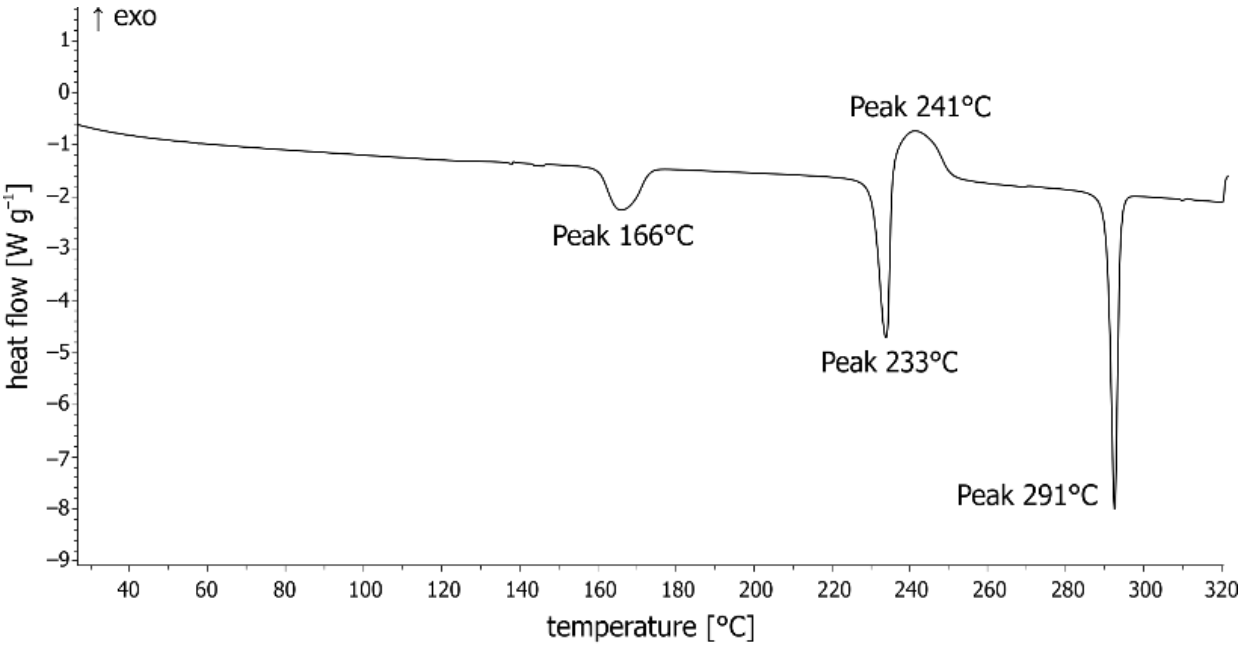
↑ exo
heat flow [W g⁻¹]
temperature [°C]
Peak 166°C
Peak 233°C
Peak 241°C
Peak 291°C

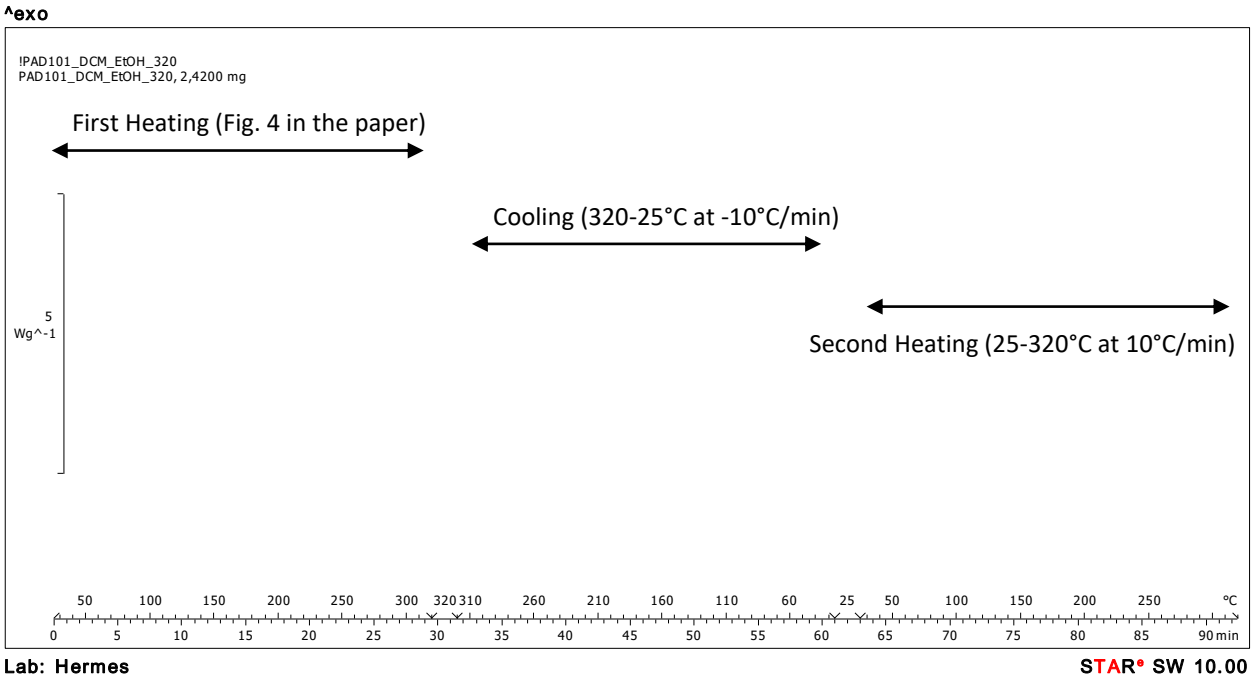

Figure S5. TTPyr(Et) crystals Top: TGA analysis; middle: DSC analysis between RT and 320°C; bottom: DSC analysis showing heating and cooling cycles.

To better investigate the thermal transformation of **TTPyr(Et)** into **TTPyr(RT)** and successively into **TTPyr(HT)**, a VT-XRPD experiment was also performed (Figure S6 and S7). Taking peaks at *ca*. 5.7, 12 and 14–14.6° as diagnostic of **TTPyr(Et)**, **TTPyr(RT)** and **TTPyr(HT)**, respectively, it is evident that DSC results are well reproduced by the VT-XRPD analysis. In particular, **TTPyr(Et)** starts to give **TTPyr(RT)** at 140°C, while the formation of **TTPyr(HT)** begins at 220°C. Comparison in the 5-15° 2θ range between calculated and experimental XRPD patterns obtained at temperatures corresponding to the complete transformation among the crystal phases is reported in Figure S6.

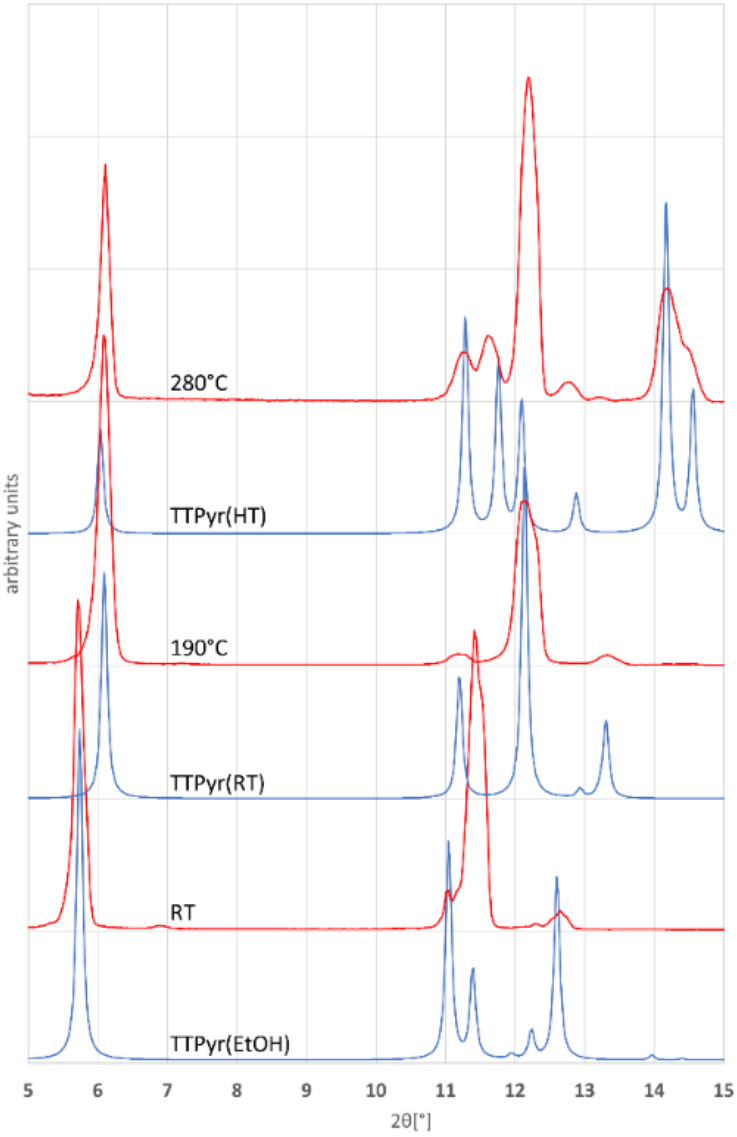

Figure S6. Comparison in the 5-15° 2θ range of calculated (blue traces) and experimental (red traces) XRPD patterns collected during the variable temperature experiment.

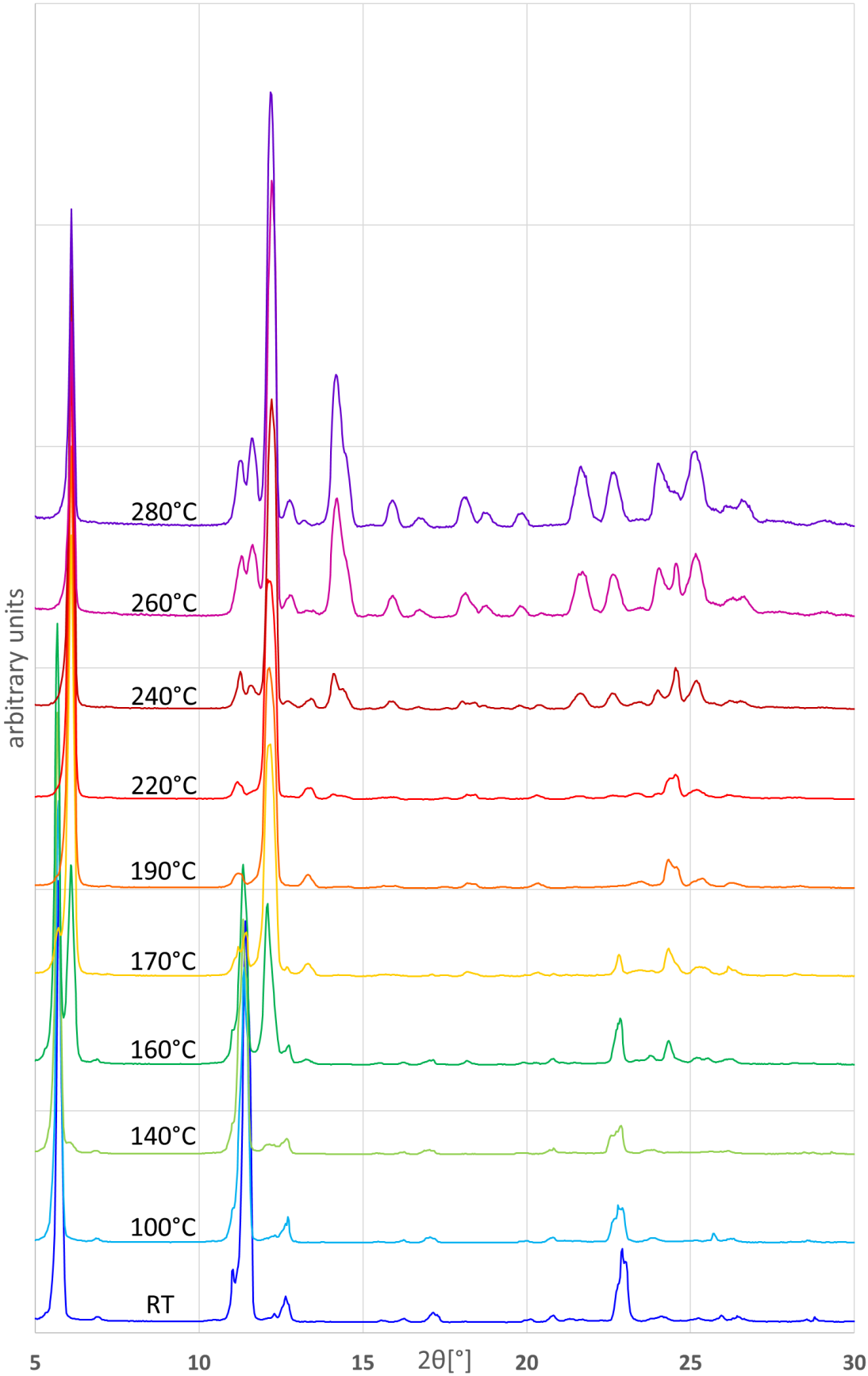

Figure S7. VT-XRPD monitoring of **TTPyr(Et)** crystals from RT to 280°C.

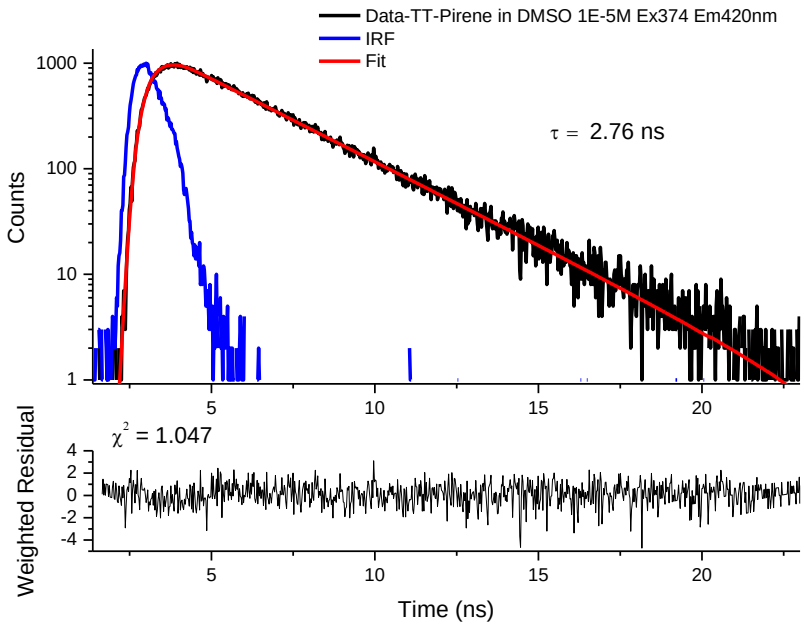

Figure S8. Lifetime measurement (λ_{exc} = 374 nm, λ_{em} = 420 nm) of **TTPyr** in DMSO at 298 K.

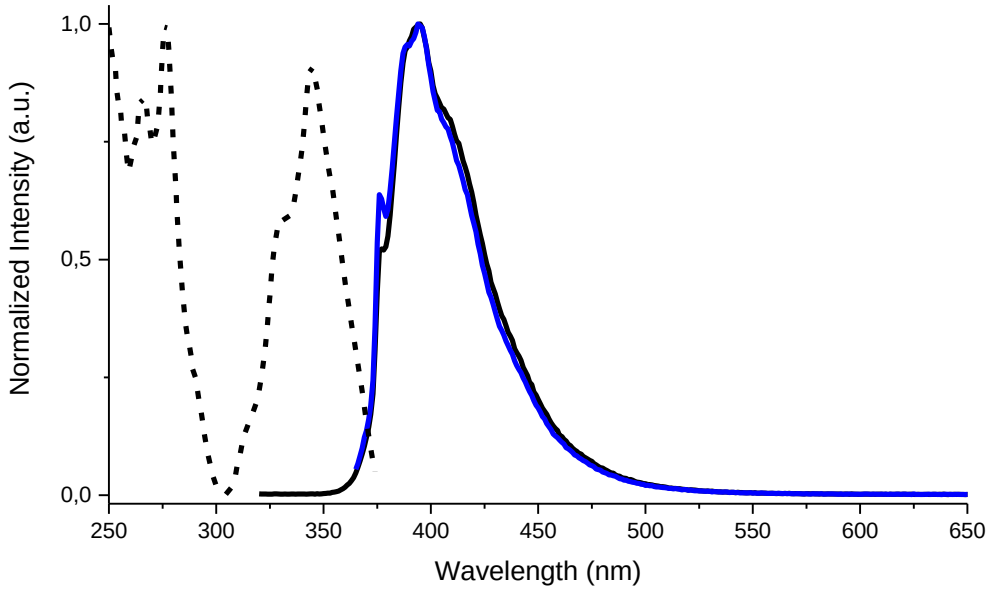

Figure S9. Normalized emission (full line) and excitation (dashed line) spectra of **TTPyr**/PMMA (0.5 % w/w) at 298 K. λ_{exc}= 300 nm (black line), λ_{exc}= 344 nm (red line); λ_{em}= 394 nm (black line).

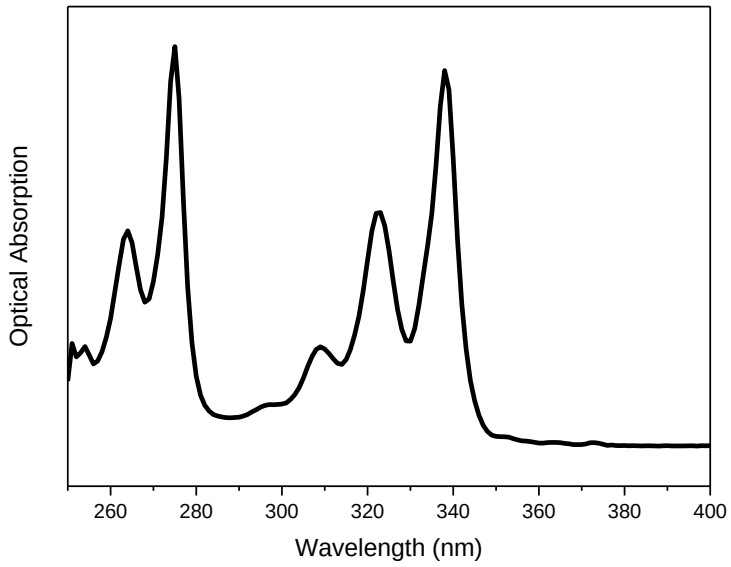

Figure S10. Absorption spectrum of pyrene in DMSO 10^{-5} M

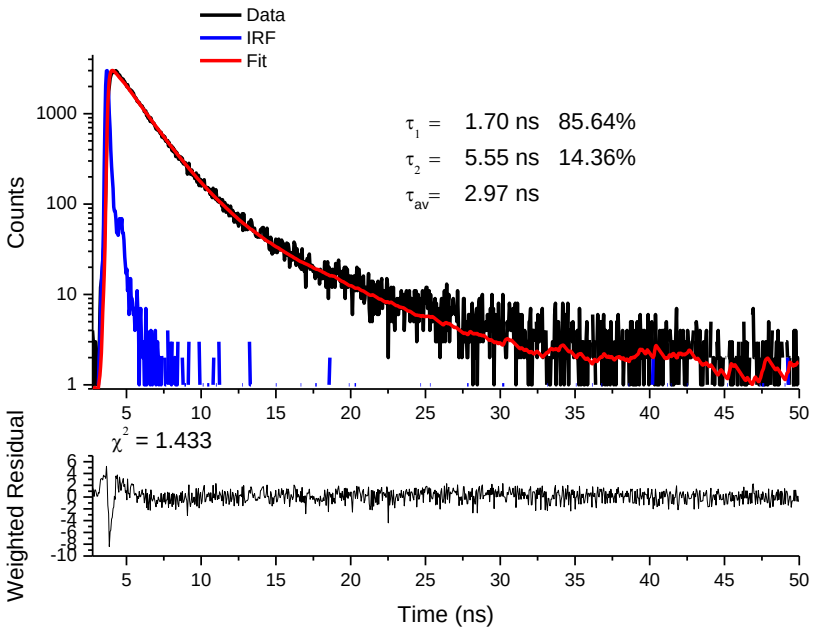

Figure S11. Lifetime measurement (λ_{exc} = 374 nm, λ_{em} = 493 nm) of **TTPyr(Et)** crystals at 298 K.

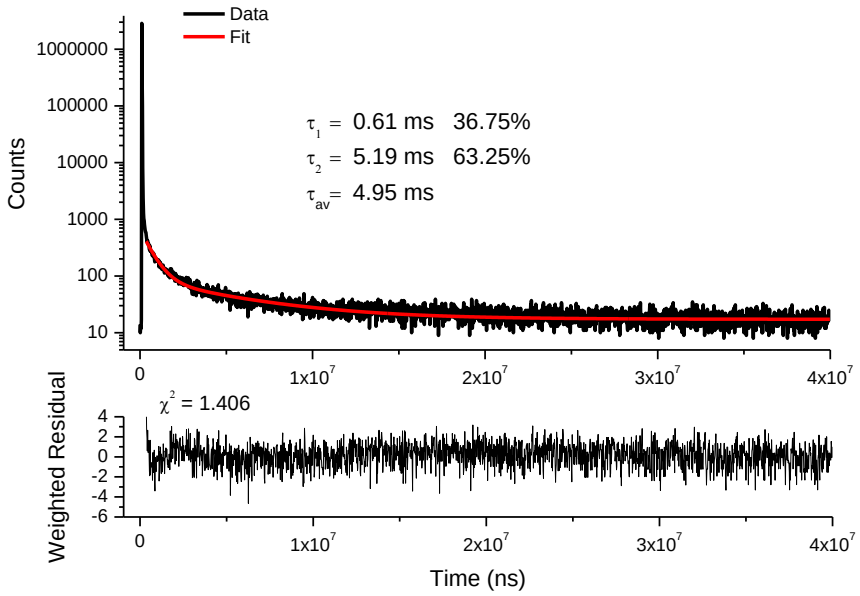

Figure S12. Lifetime measurement (λ_{exc} = 374 nm, λ_{em} = 555 nm) of **TTPyr(Et)** crystals at 298 K.

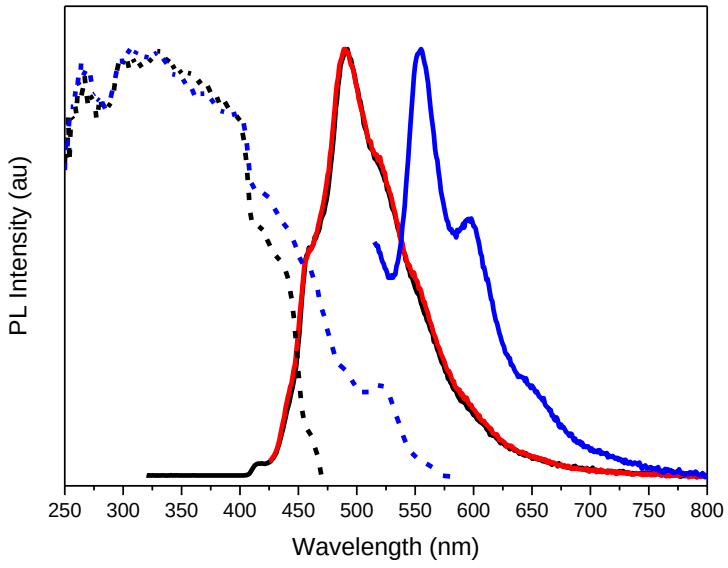

Figure S13. Normalized emission (full line) and excitation (dashed line) spectra of **TTPyr(Et)** crystals at 77 K. λ_{exc}= 300 nm (black line), λ_{exc}= 405 nm (red line), λ_{exc}= 495 nm (blue line); λ_{em}= 491 nm (black line), λ_{em}= 617 nm (blue line).

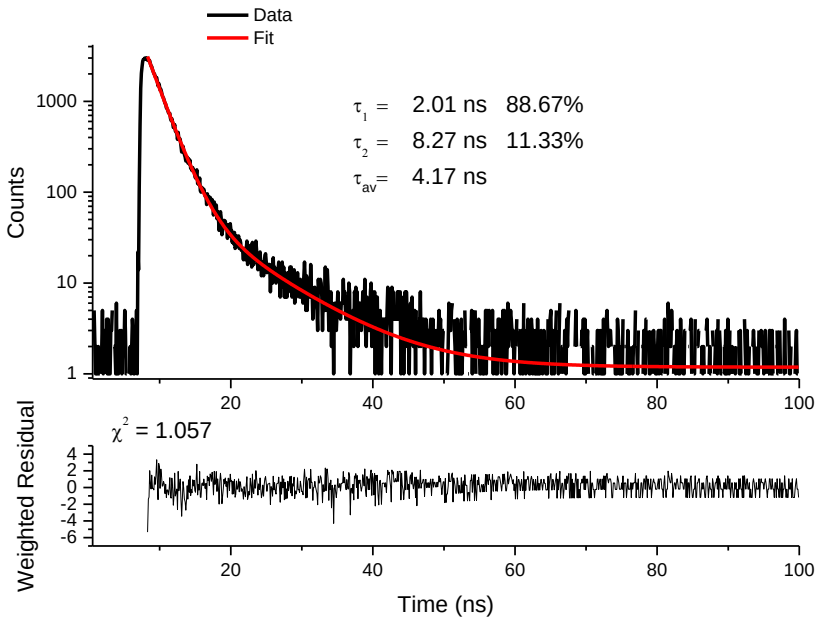

Figure S14. Lifetime measurement (λ_{exc} = 374 nm, λ_{em} = 493 nm) of **TTPyr(Et)** crystals at 77 K.

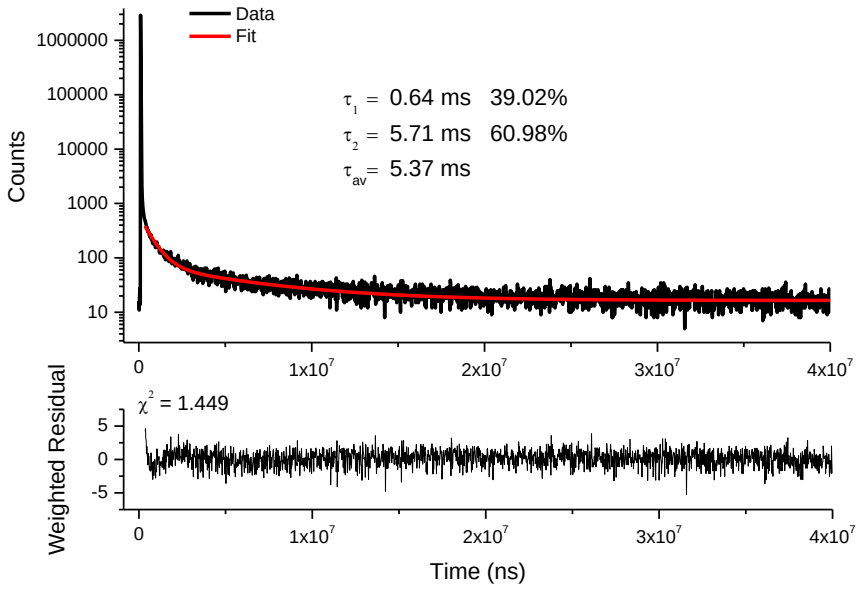

Figure S15. Lifetime measurement (λ_{exc} = 374 nm, λ_{em} = 555 nm) of **TTPyr(Et)** crystals at 77 K.

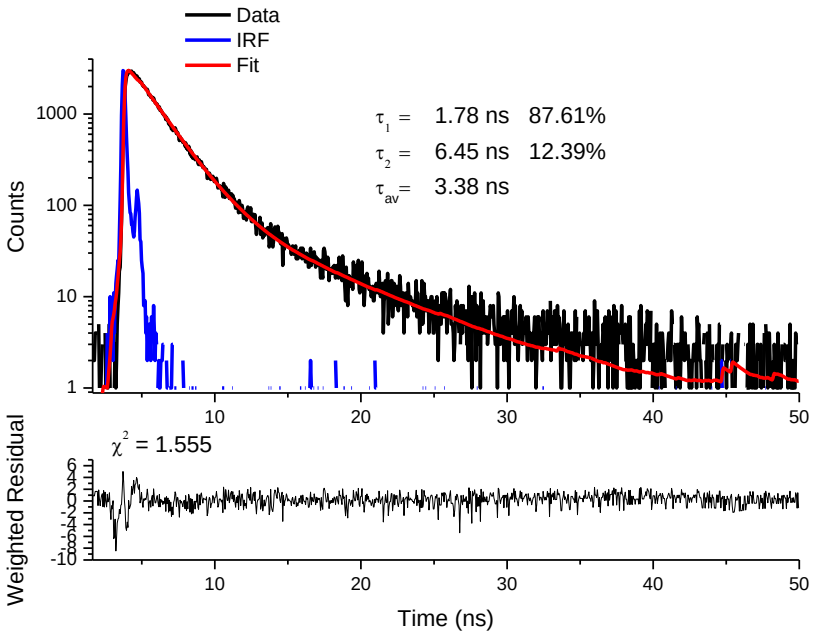

Figure S16. Lifetime measurement (λ_{exc} = 374 nm, λ_{em} = 493 nm) of **TTPyr(Me)** crystals at 298 K.

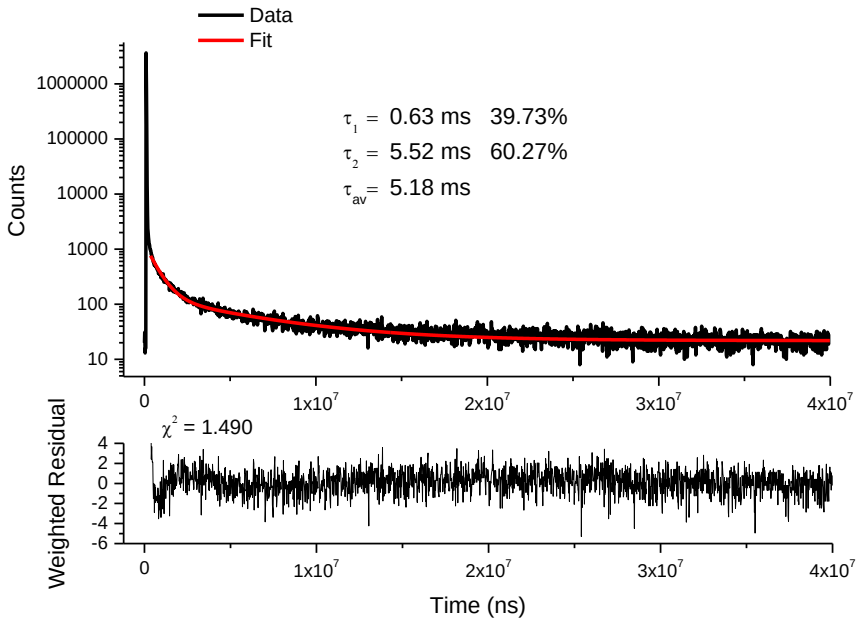

Figure S17. Lifetime measurement (λ_{exc} = 374 nm, λ_{em} = 550 nm) of **TTPyr(Me)** crystals at 298 K.

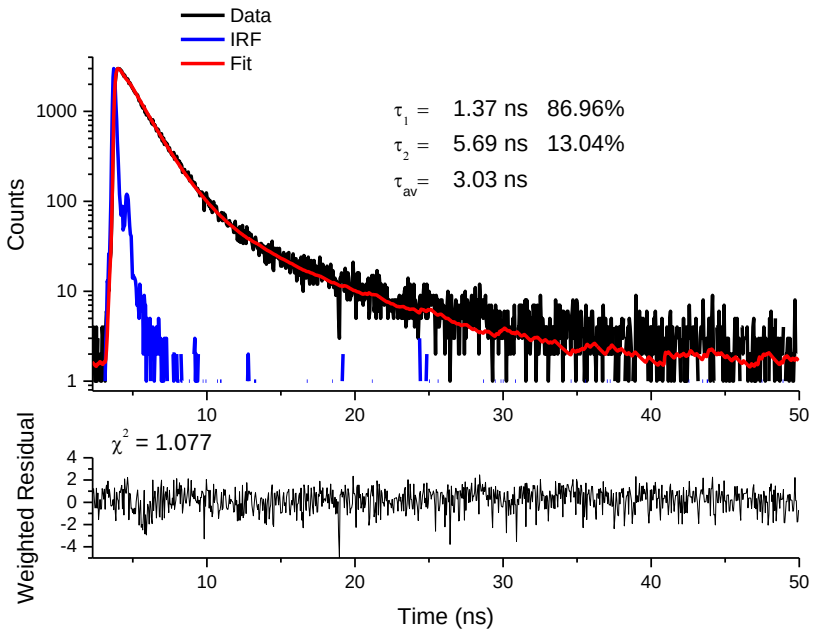

Figure S18. Lifetime measurement (λ_{exc} = 374 nm, λ_{em} = 490 nm) of **TTPyr(RT)-small** crystals at 298 K.

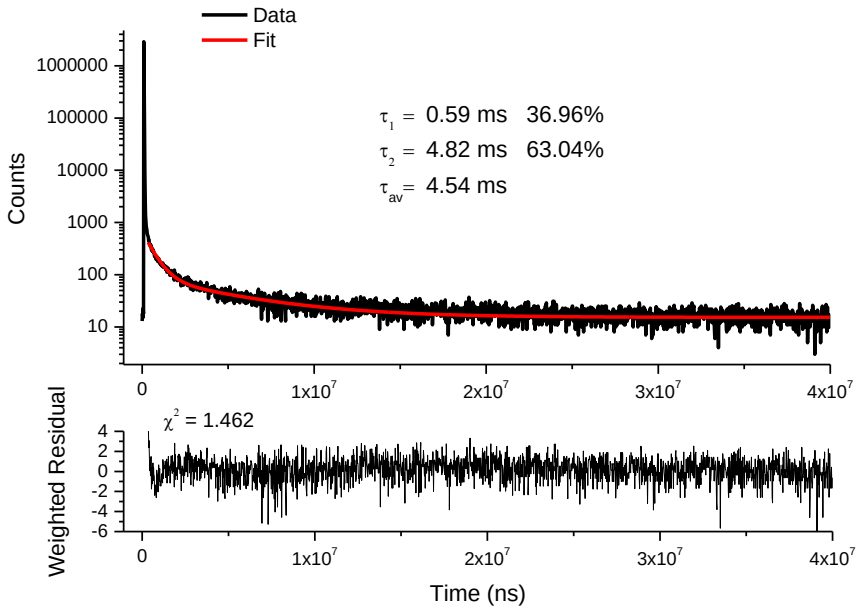

Figure S19. Lifetime measurement (λ_{exc} = 374 nm, λ_{em} = 550 nm) of **TTPyr(RT)-small** crystals at 298 K.

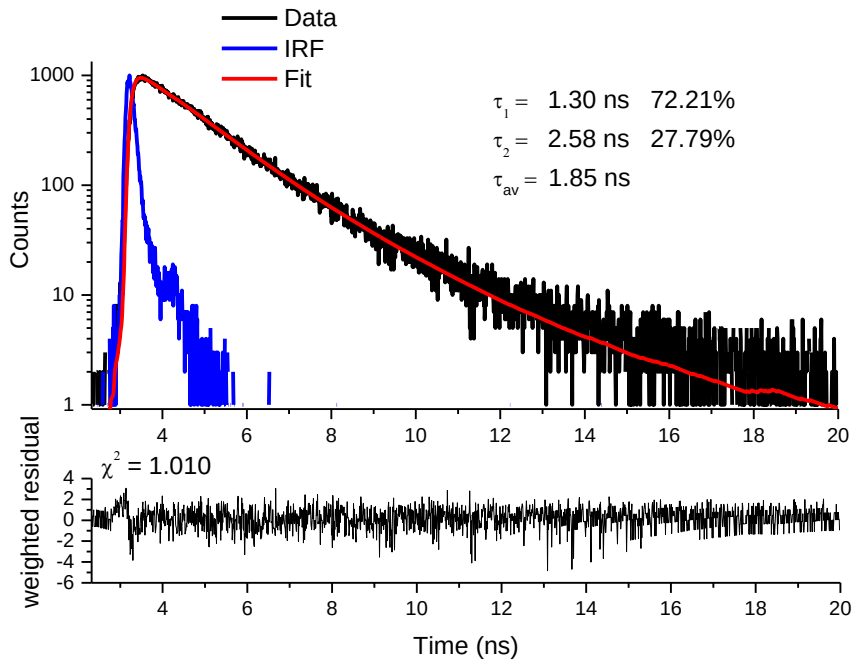

Figure S20. Lifetime measurement (λ_{exc} = 374 nm, λ_{em} = 467 nm) of **TTPyr(RT)-large** crystals at 298 K.

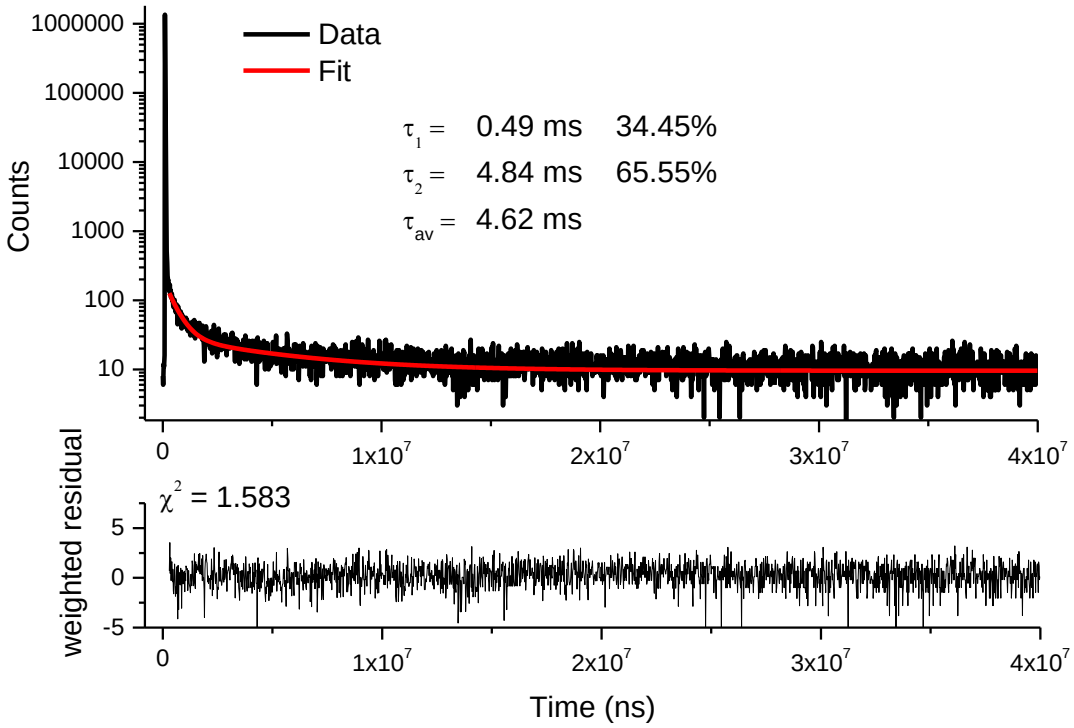

Figure S21. Lifetime measurement (λ_{exc} = 374 nm, λ_{em} = 553 nm) of **TTPyr(RT)-large** crystals at 298 K.

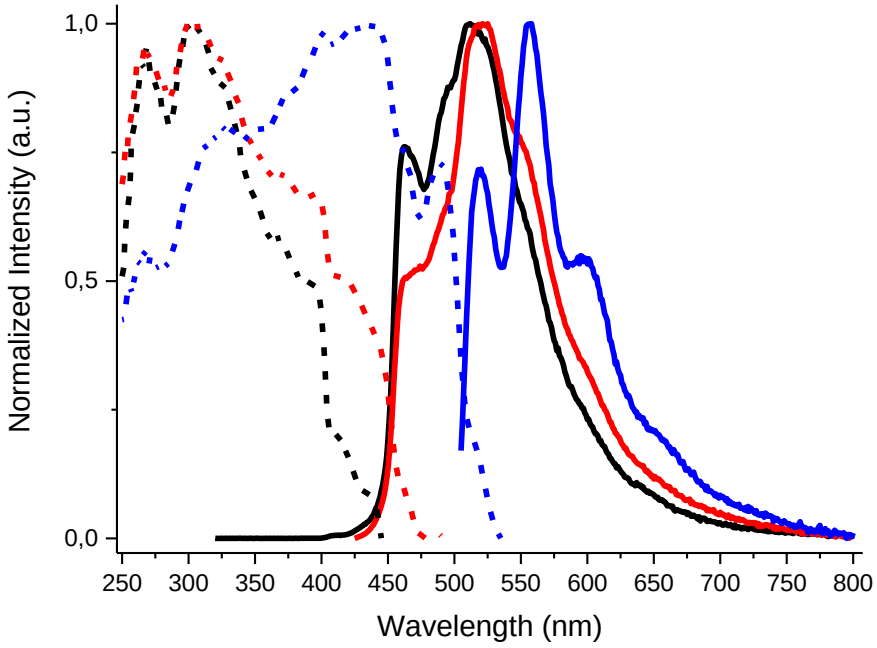

Figure S22. Normalized emission (full line) and excitation (dashed line) spectra of **TTPyr(RT)-large** crystals at 77 K. λ_{exc}= 300 nm (black line), λ_{exc}= 405 nm (red line), λ_{exc}= 490 nm (blue line); λ_{em}= 463 nm (black line), λ_{em}= 511 nm (red line), λ_{em}= 557 nm (blue line).

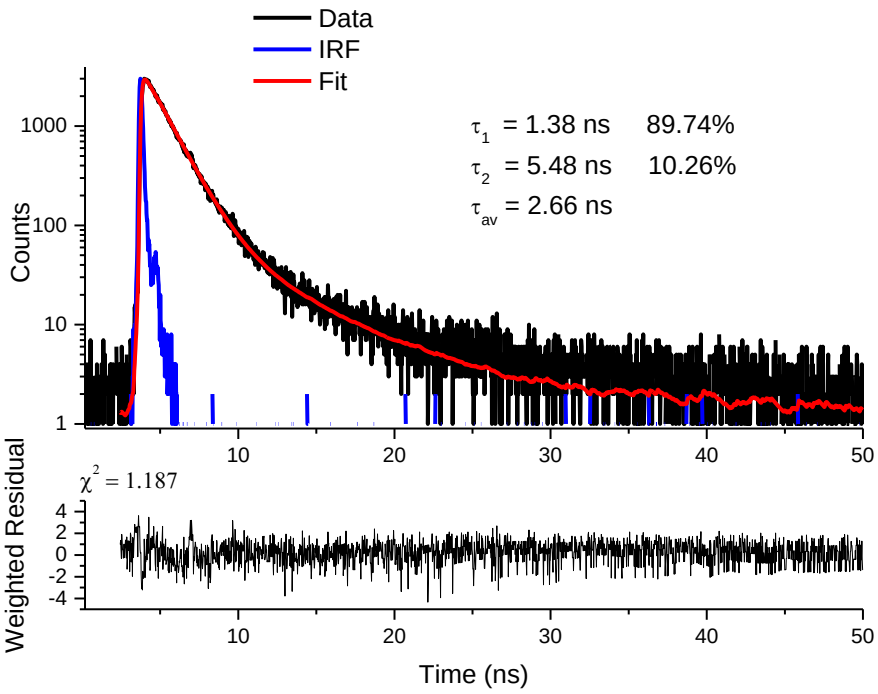

Figure S23. Lifetime measurement (λ_{exc} = 374 nm, λ_{em} = 463 nm) of **TTPyr(RT)-large** crystals at 77 K.

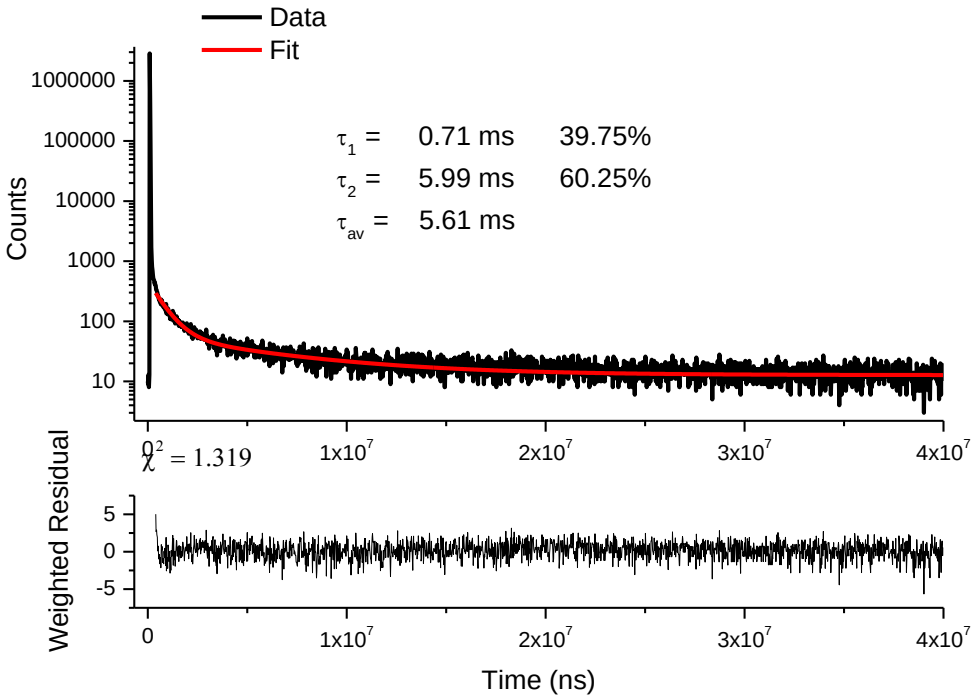

Figure S24. Lifetime measurement (λ_{exc} = 374 nm, λ_{em} = 557 nm) of **TTPyr(RT)-large** crystals at 77 K.

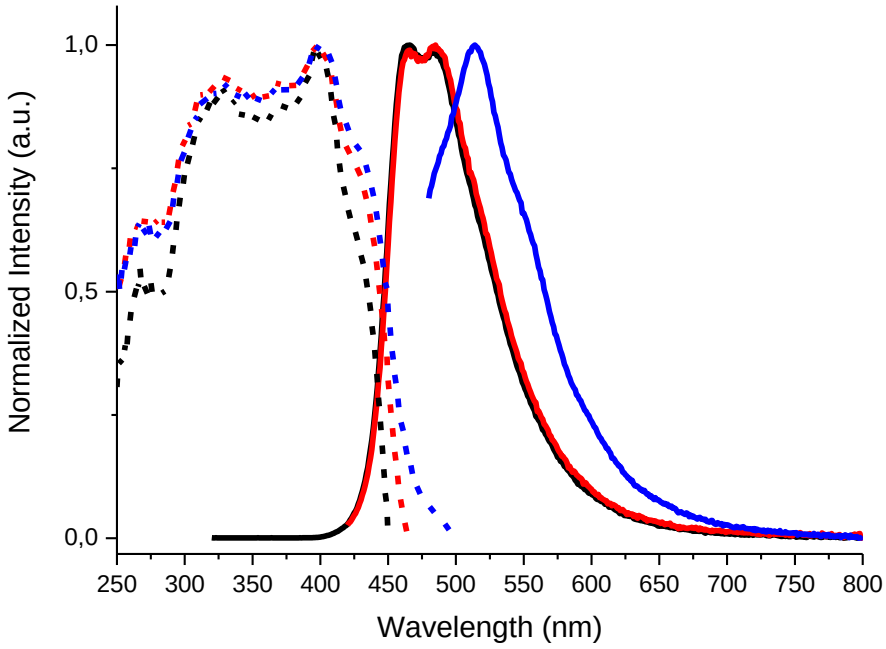

Figure S25. Normalized emission (full line) and excitation (dashed line) spectra of **TTPyr(RT)-ground** crystals at 298 K. λ_{exc}= 300 nm (black line), λ_{exc}= 405 nm (red line), λ_{exc}= 460 nm (blue line); λ_{em}= 465 nm (black line), λ_{em}= 484 nm (red line), λ_{em}= 514 nm (blue line).

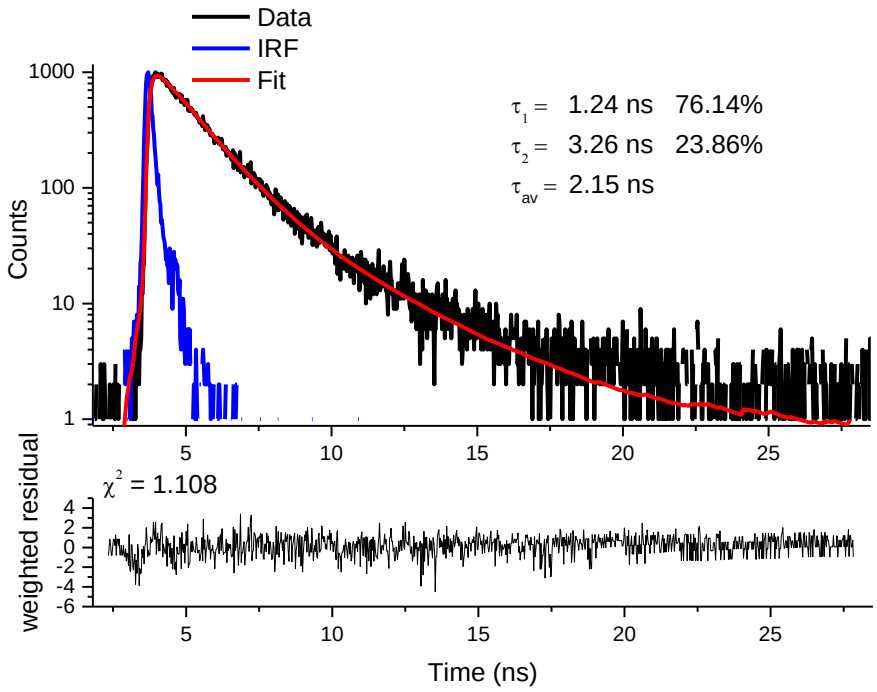

Figure S26. Lifetime measurement (λ_{exc} = 374 nm, λ_{em} = 463 nm) of **TTPyr(RT)-ground** crystals at 298 K.

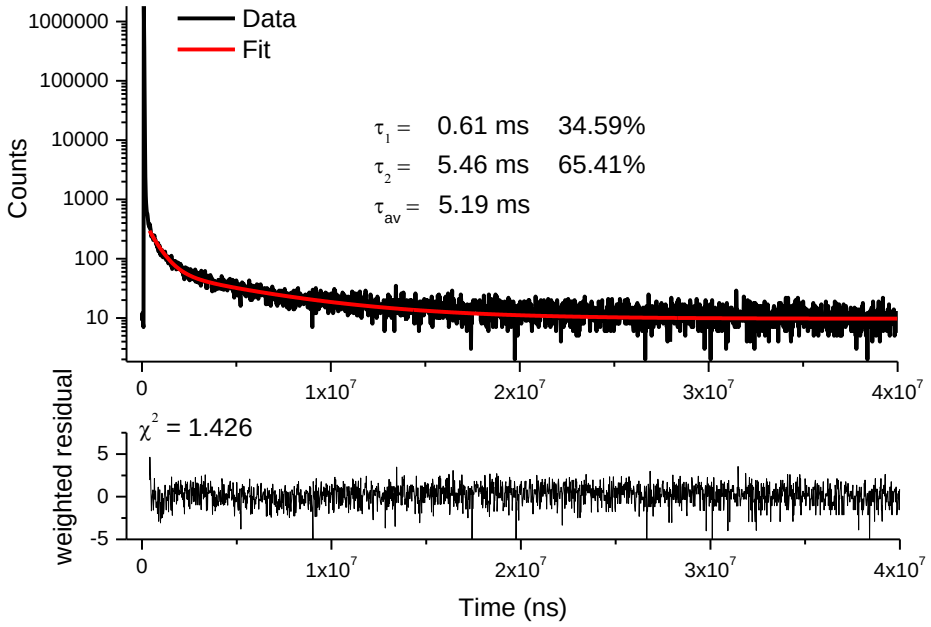

Figure S27. Lifetime measurement (λ_{exc} = 374 nm, λ_{em} = 514 nm) of **TTPyr(RT)-ground** crystals at 298 K.

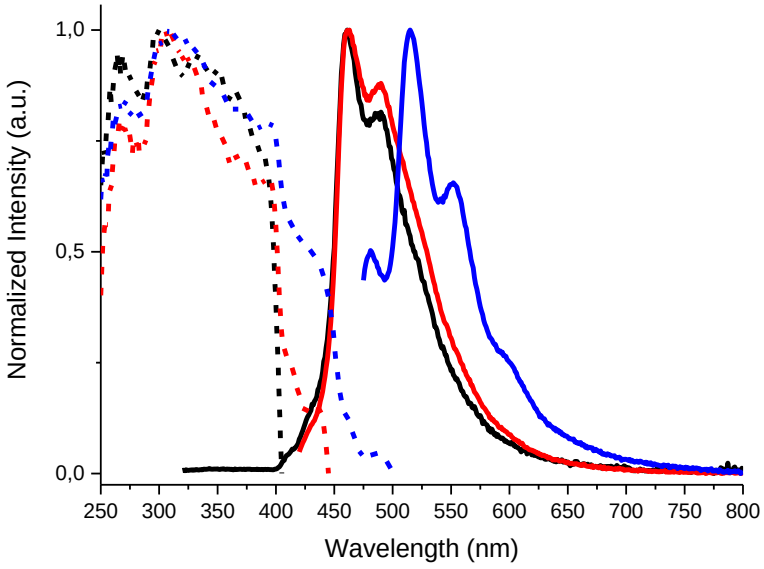

Figure S28. Normalized emission (full line) and excitation (dashed line) spectra of **TTPyr(RT)-ground** crystals at 77 K. λ_{exc}= 300 nm (black line), λ_{exc}= 405 nm (red line), λ_{exc}= 460 nm (blue line); λ_{em}= 420 nm (black line), λ_{em}= 461 nm (red line), λ_{em}= 515 nm (blue line).

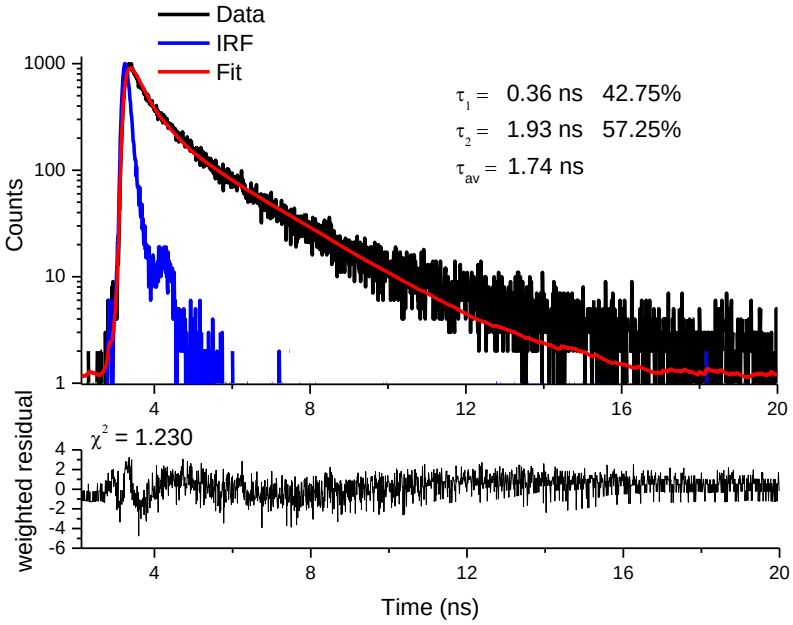

Figure S29. Lifetime measurement (λ_{exc} = 374 nm, λ_{em} = 420 nm) of **TTPyr(RT)-ground** crystals at 77 K.

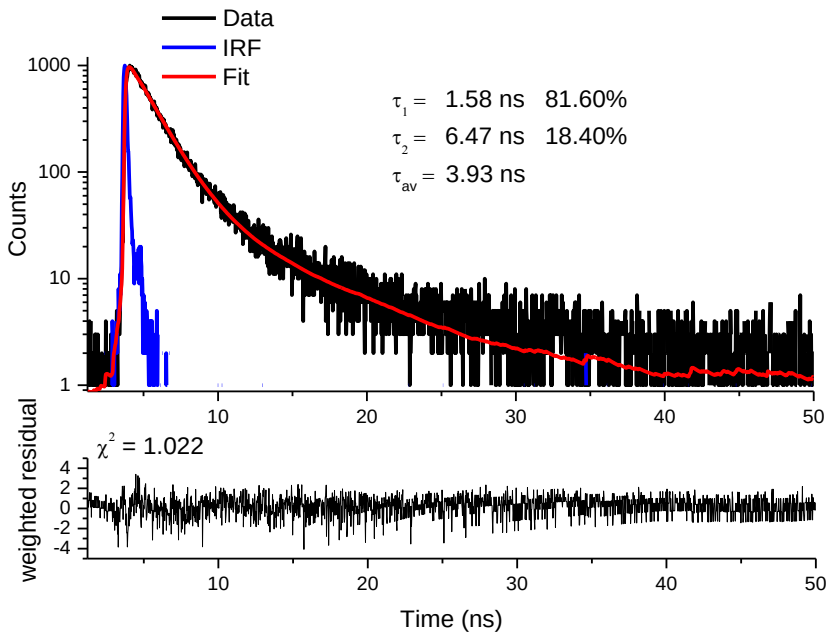

Figure S30. Lifetime measurement (λ_{exc} = 374 nm, λ_{em} = 461 nm) of **TTPyr(RT)-ground** crystals at 77 K.

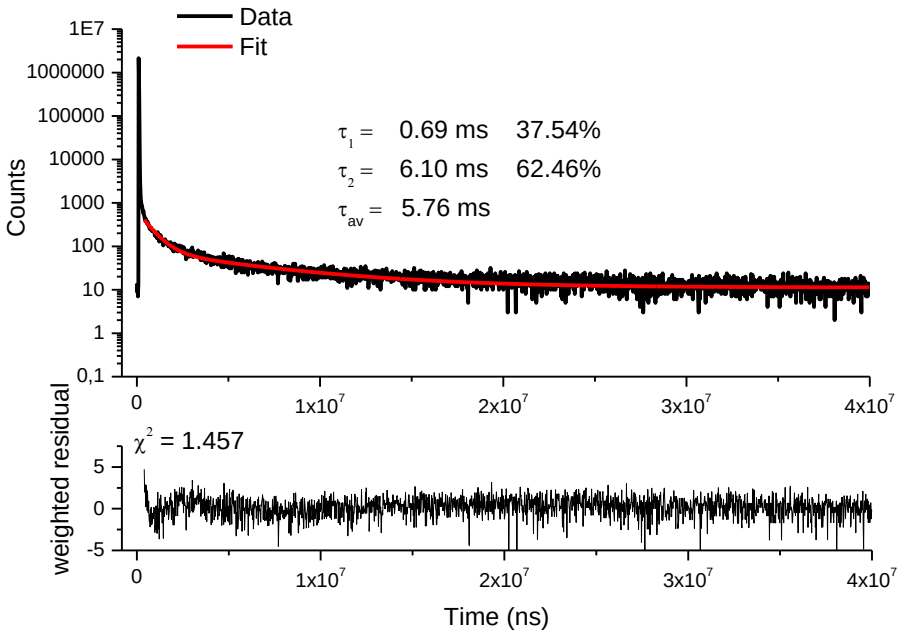

Figure S31. Lifetime measurement (λ_{exc} = 374 nm, λ_{em} = 515 nm) of **TTPyr(RT)-ground** crystals at 77 K.

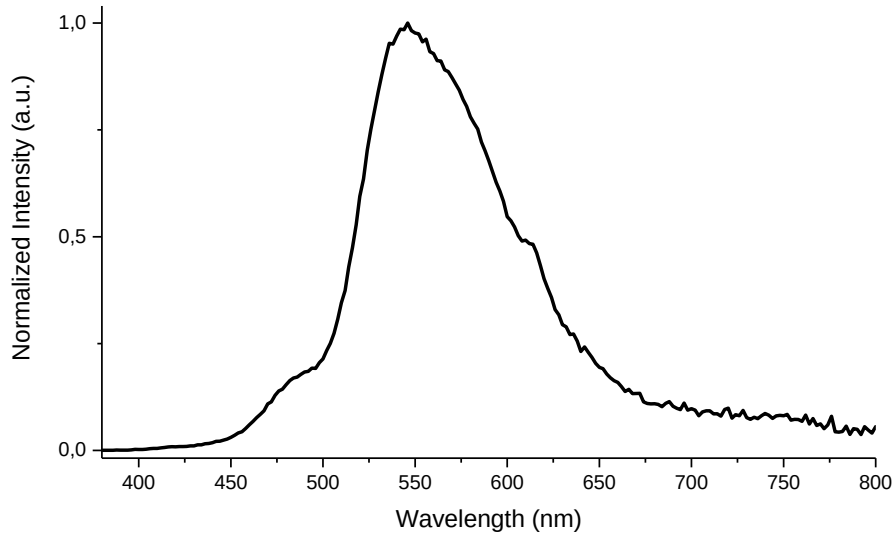

Figure S32. Delayed Emission spectrum of **TTPyr(HT)** polycrystalline phase prepared from **TTPyr(Et)** crystals at 298 K. Excitation at 300 nm, delay 100 μs, window 200 μs

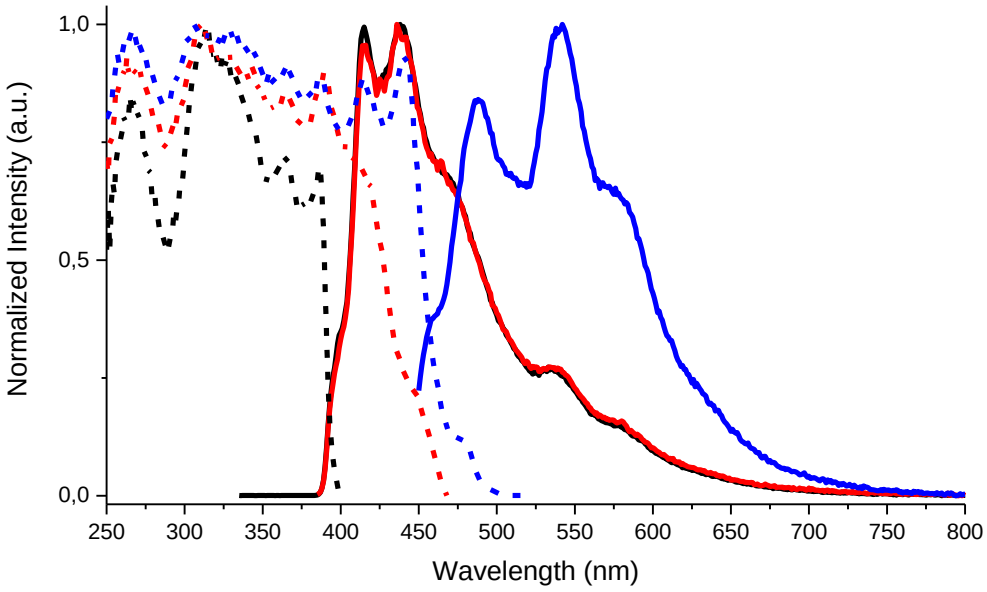

Figure S33. Normalized emission (full line) and excitation (dashed line) spectra at 77 K of **TTPyr(HT)** polycrystalline phase prepared from **TTPyr(Et)** crystals. λ_{exc}= 315 nm (black line), λ_{exc}= 370 nm (red line), λ_{exc}= 437 nm (blue line); λ_{em}= 415 nm (black line), λ_{em}= 488 nm (red line), λ_{em}= 540 nm (blue line).

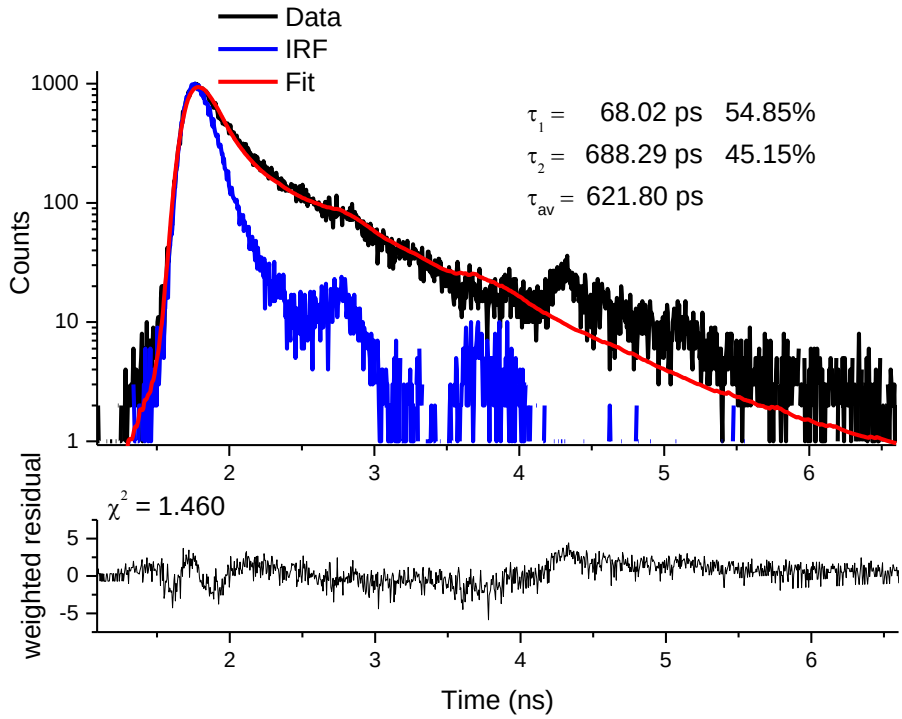

Figure S34. Lifetime measurement (λ_{exc} = 374 nm, λ_{em} = 415 nm) at 298 K of **TTPyr(HT)** polycrystalline phase prepared from **TTPyr(RT)-large** crystals.

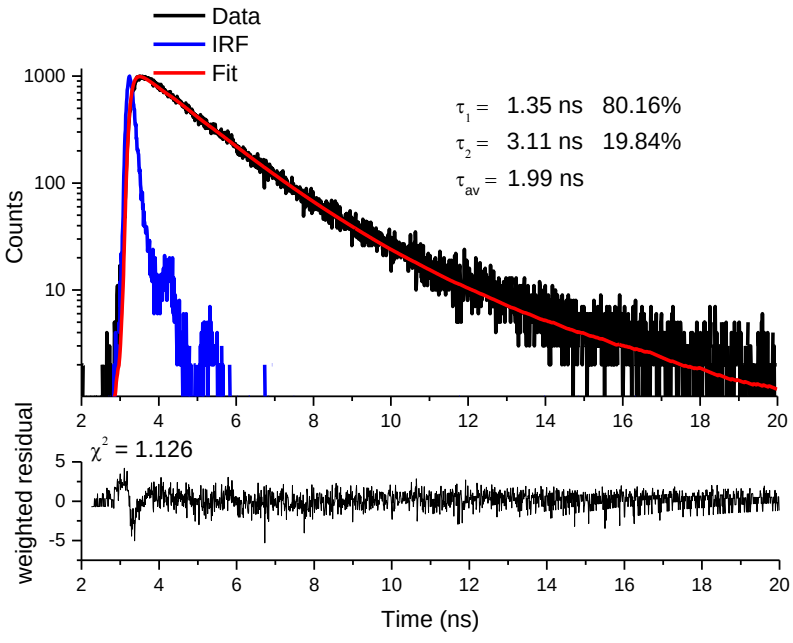

Figure S35. Lifetime measurement (λ_{exc} = 374 nm, λ_{em} = 480 nm) at 298 K of **TTPyr(HT)** polycrystalline phase prepared from **TTPyr(RT)-large** crystals.

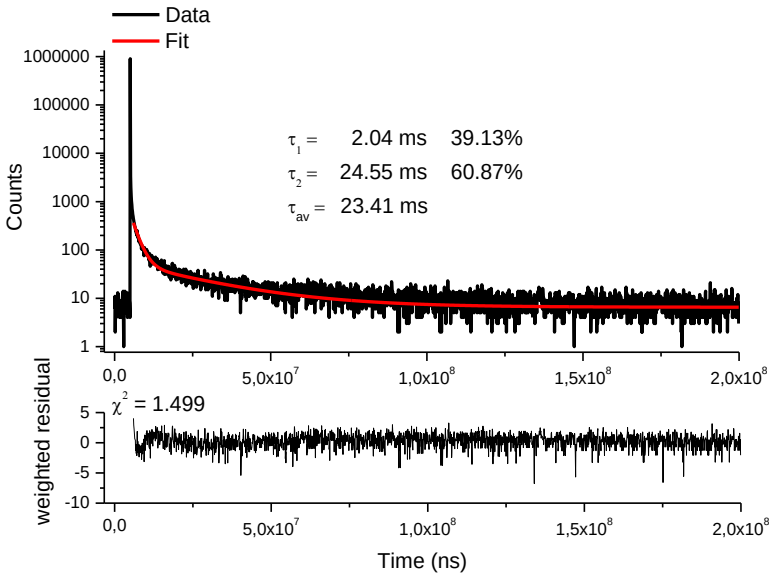

Figure S36. Lifetime measurement (λ_{exc} = 374 nm, λ_{em} = 550 nm) at 298 K of **TTPyr(HT)** polycrystalline phase prepared from **TTPyr(RT)-large** crystals.

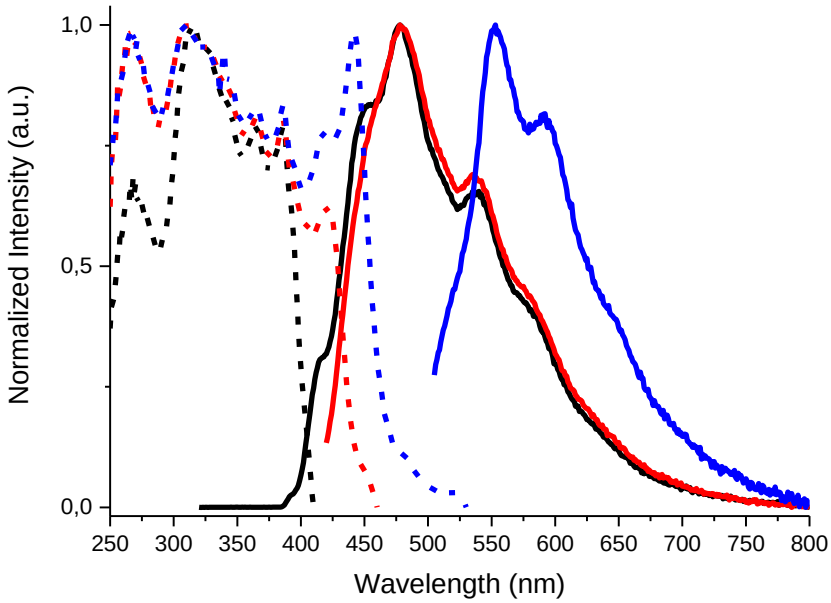

Figure S37. Normalized emission (full line) and excitation (dashed line) spectra at 77 K of **TTPyr(HT)** polycrystalline phase prepared from **TTPyr(RT)-large** crystals. λ_{exc}= 300 nm (black line), λ_{exc}= 405 nm (red line), λ_{exc}= 490 nm (blue line); λ_{em}= 430 nm (black line), λ_{em}= 480 nm (red line), λ_{em}= 552 nm (blue line).

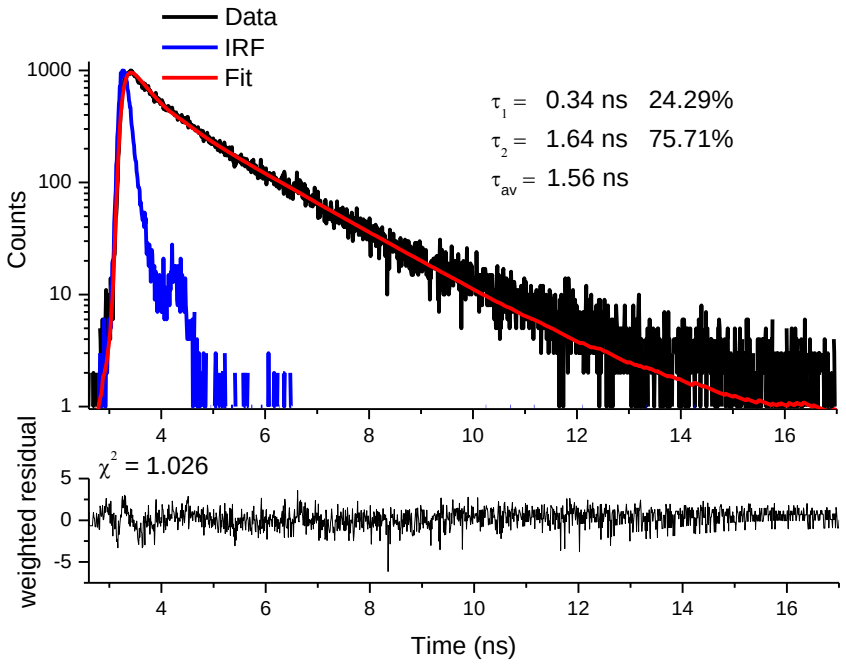

Figure S38. Lifetime measurement (λ_{exc} = 374 nm, λ_{em} = 415 nm) at 77 K of **TTPyr(HT)** polycrystalline phase prepared from **TTPyr(RT)-large** crystals.

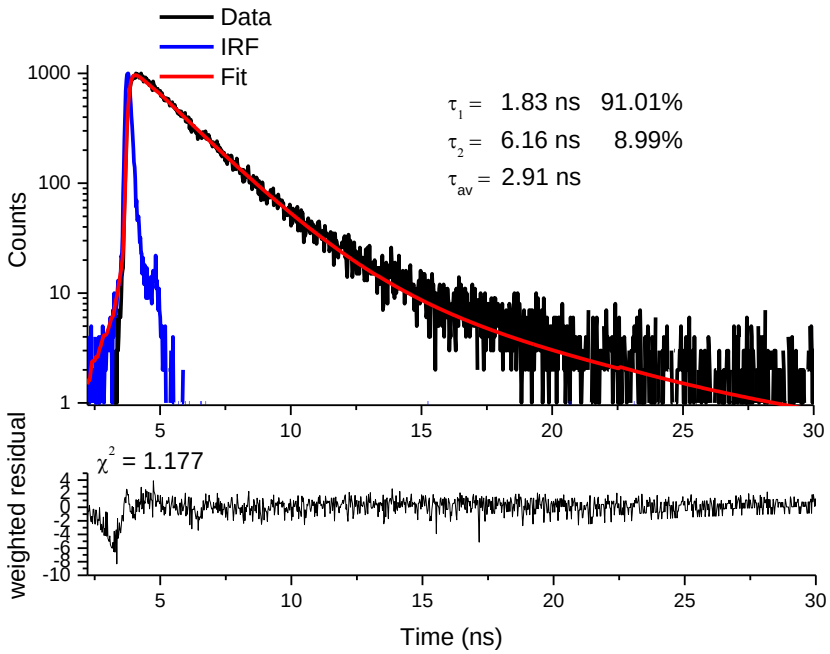

Figure S39. Lifetime measurement (λ_{exc} = 374 nm, λ_{em} = 480 nm) at 77 K of **TTPyr(HT)** polycrystalline phase prepared from **TTPyr(RT)-large** crystals.

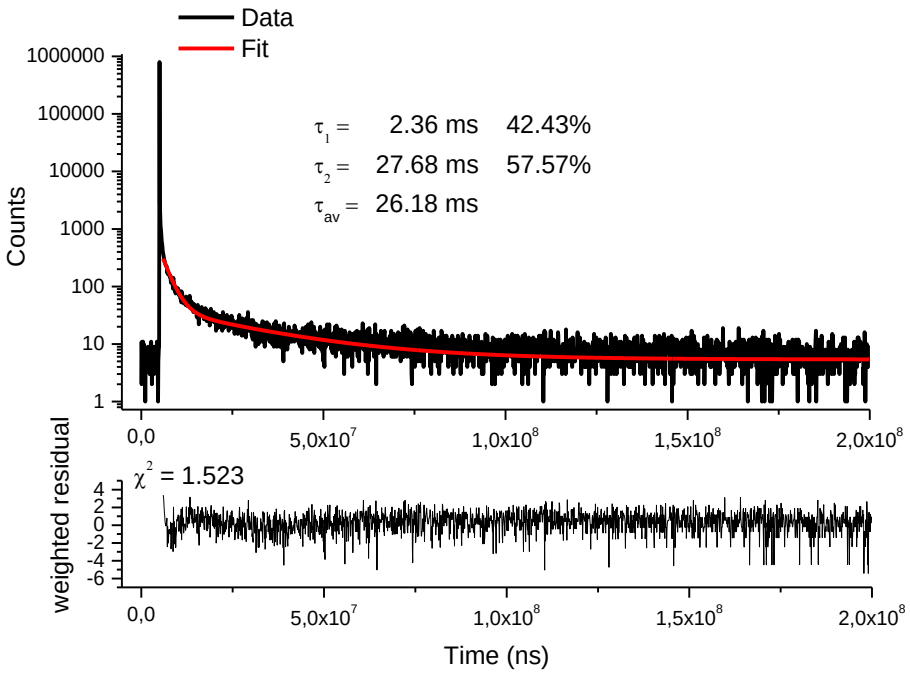

Figure S40. Lifetime measurement (λ_{exc} = 374 nm, λ_{em} = 552 nm) at 77 K of **TTPyr(HT)** polycrystalline phase prepared from **TTPyr(RT)-large** crystals.

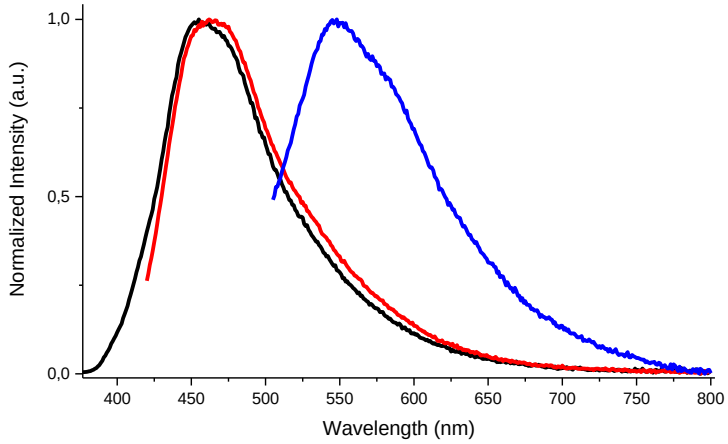

Figure S41. Normalized emission spectra at 298 K of ground **TTPyr(HT)** polycrystalline phase prepared from **TTPyr(RT)-large** crystals. λ_{exc}= 300 nm (black line), λ_{exc}= 405 nm (red line), λ_{exc}= 490 nm (blue line).

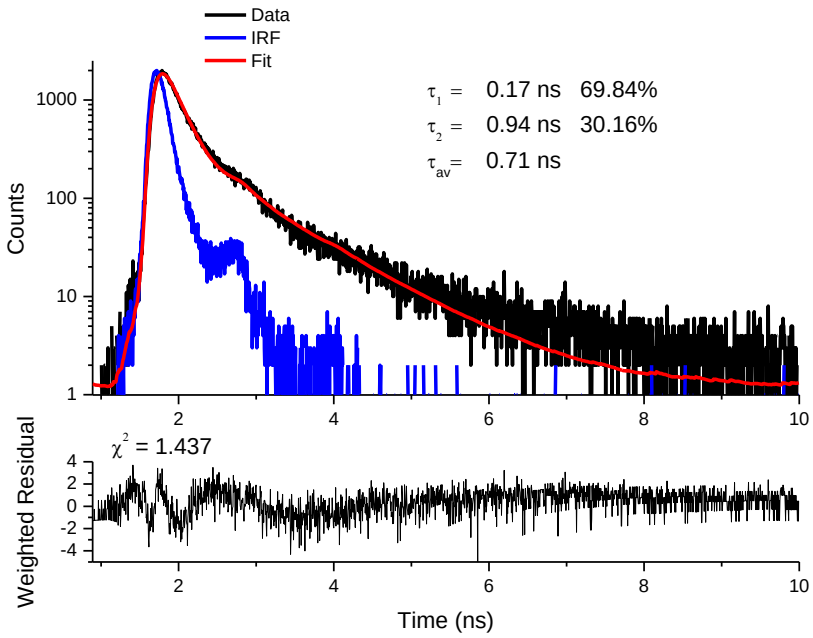

Figure S42. Lifetime measurement (λ_{exc} = 374 nm, λ_{em} = 415 nm) at 298 K of ground **TTPyr(HT)** polycrystalline phase prepared from **TTPyr(RT)-large** crystals.

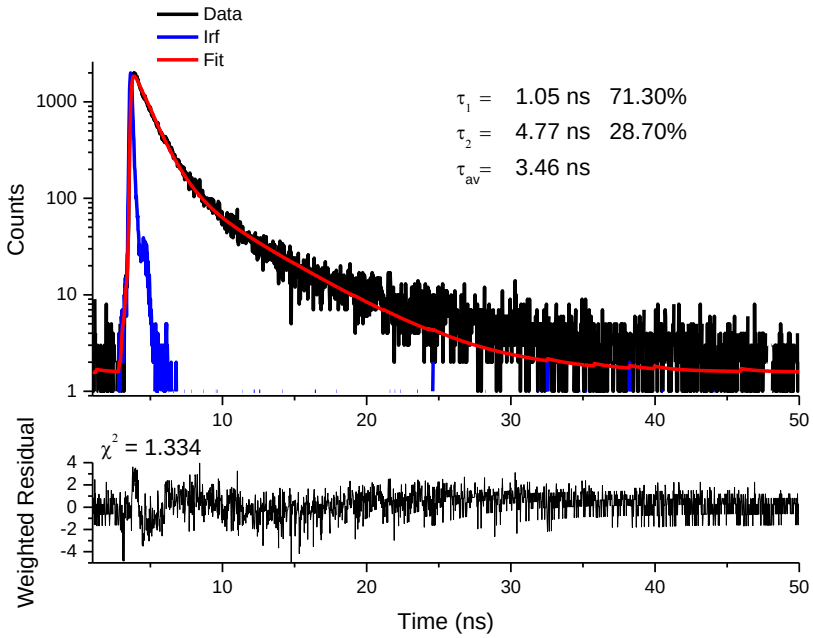

Figure S43. Lifetime measurement (λ_{exc} = 374 nm, λ_{em} = 481 nm) at 298 K of ground **TTPyr(HT)** polycrystalline phase prepared from **TTPyr(RT)-large** crystals.

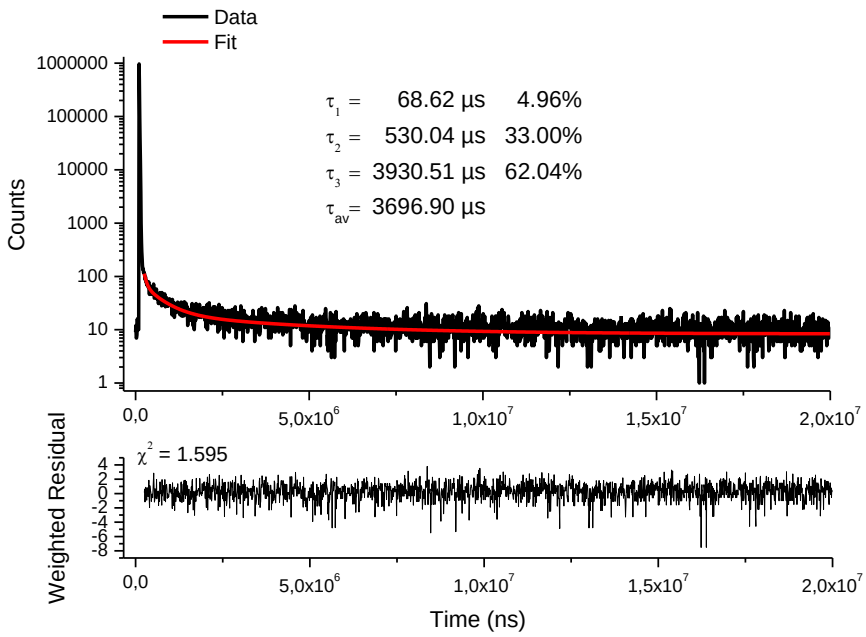

Figure S44. Lifetime measurement (λ_{exc} = 374 nm, λ_{em} = 550 nm) at 298 K of ground **TTPyr(HT)** polycrystalline phase prepared from **TTPyr(RT)-large** crystals.

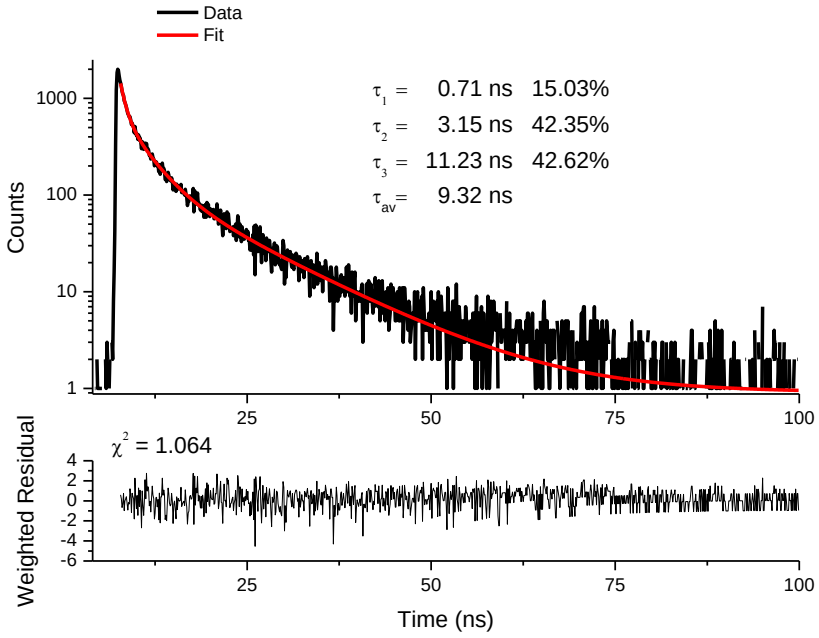

Figure S45. Lifetime measurement (λ_{exc} = 374 nm, λ_{em} = 468 nm) at 298 K of **TTPyr** amorphous film.

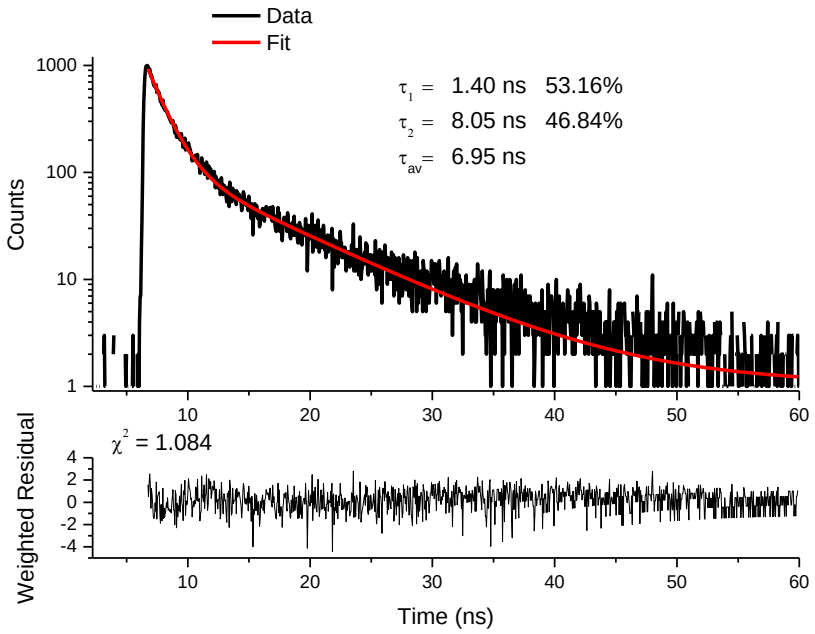

Figure S46. Lifetime measurement (λ_{exc} = 405 nm, λ_{em} = 462 nm) at 298 K of pristine **TTPyr** cast film.

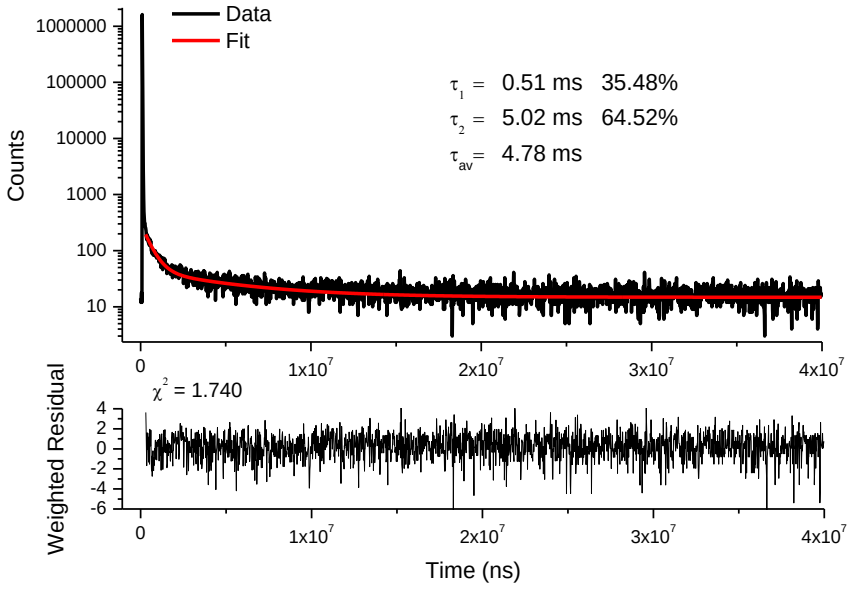

Figure S47. Lifetime measurement (λ_{exc} = 405 nm, λ_{em} = 505 nm) at 298 K of pristine **TTPyr** cast film.

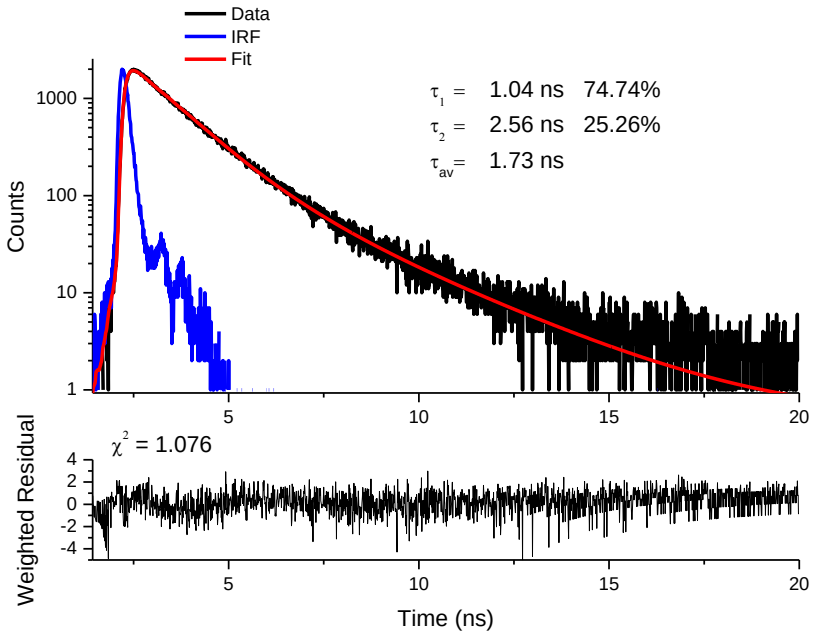

Figure S48. Lifetime measurement (λ_{exc} = 405 nm, λ_{em} = 462 nm) at 298 K of **TTPyr** cast film heated at 220°C for 90 min.

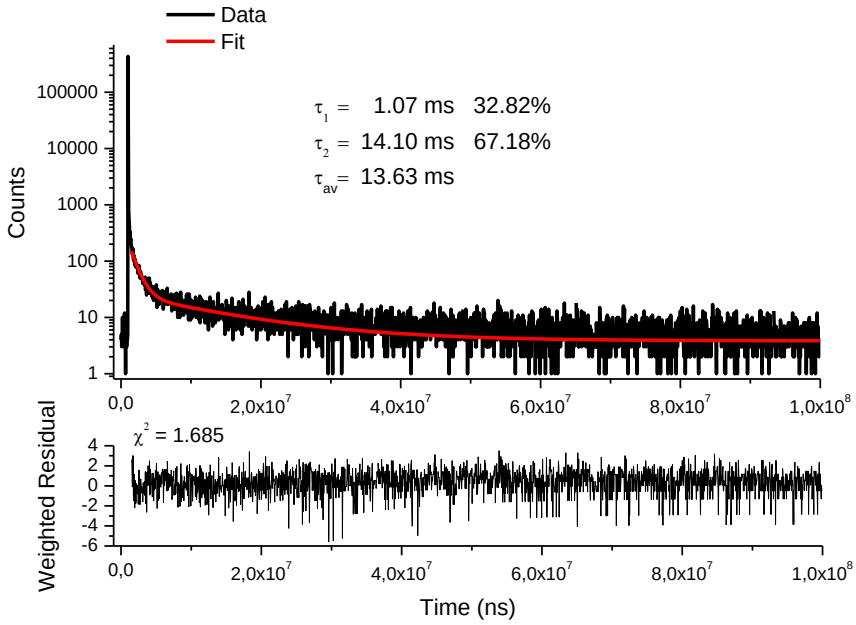

Figure S49. Lifetime measurement (λ_{exc} = 405 nm, λ_{em} = 505 nm) at 298 K of **TTPyr** cast film heated at 220°C for 90 min.

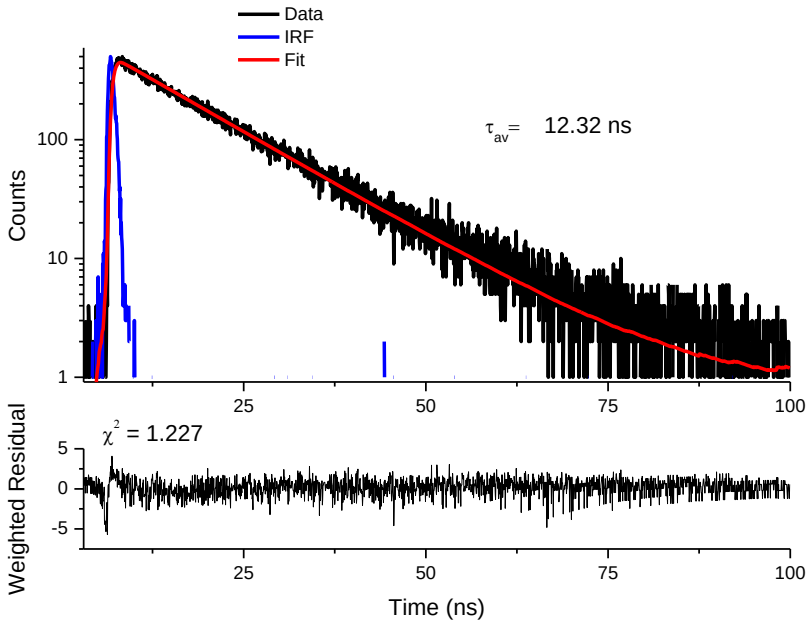

Figure S50. Lifetime measurement (λ_{exc} = 300 nm, λ_{em} = 398 nm) of **TTPyr** in H_2O/DMSO (90/10 w/w) at 298 K.

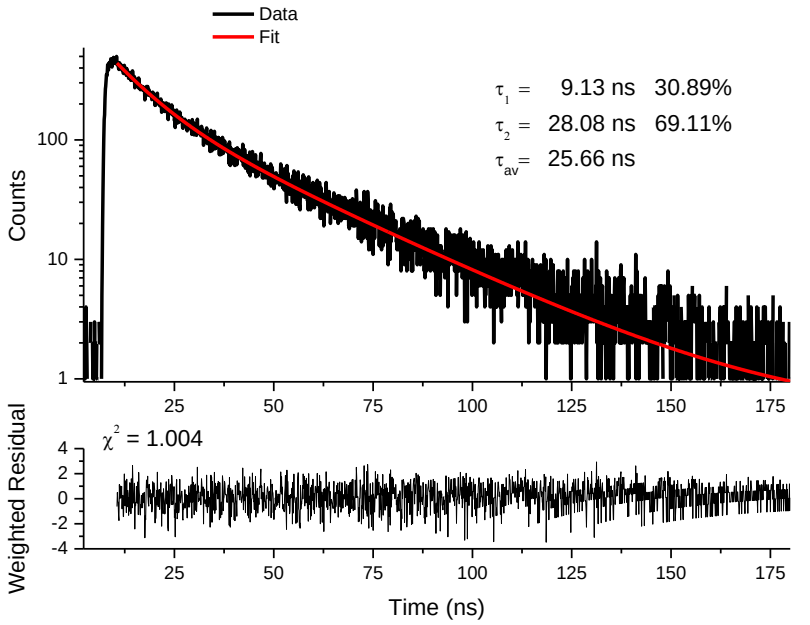

Figure S51. Lifetime measurement (λ_{exc} = 300 nm, λ_{em} = 480 nm) of **TTPyr** in H_2O/DMSO (90/10 w/w) at 298 K.

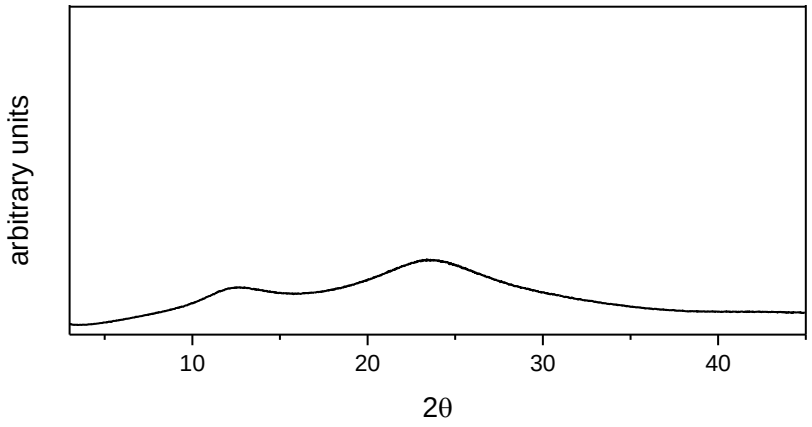

Figure S52. XRPD pattern of **TTPyr** amorphous film.

1.7. Biological imaging experiments.

Cell Imaging and Confocal Colocalization:

HeLa cells and HLF cells were cultured in the Dulbecco's Modified Eagle Medium (DMEM) containing 10 % fetal bovine serum (FBS) and antibiotics (100 units/mL penicillin and 100 mg/mL streptomycin) in a 5% CO_2 humidity incubator at 37 °C. After cells were incubated with TTPyr and the commercial probes at 37 °C for 30 min, the medium was removed and the cells were rinsed with phosphate buffer saline (PBS) three times and then imaged under a confocal microscope (ZEISS, LSM800). The excitation was 405 nm for TTPyr, 488 nm for Lyso-Tracker Green DND 26, 488 nm for BODIPY 493/503 and 633 nm for Mito-Tracker Deep Red.

Cytotoxicity Study:

Cells were seeded in 96-well plates (Costar, IL, U.S.A.) at a density of 5000 cells/well. After overnight culturing, the medium in each well were replaced by 100 µL of fresh medium containing different concentrations of TTPyr. After 24 h incubation, 10 µL of MTT solution (5 mg/mL in PBS) was added into each well and incubated for 4 h, 100 µL of DMSO was added to each well and then vibrated for 15 min. The absorption of each well at 595 nm was recorded via a plate reader (Varioskan LUX multimode microplate reader). Each trial was performed with 6 wells parallel.

Bacteria culture and imaging:

A single colony of bacteria on solid culture medium was transferred to 5 mL of liquid culture medium (Luria-Bertani (LB) Broth) and grown at 37 °C for 10 h. After reaching logarithmic phase, 500 µL of bacteria was transferred to a 1.5 mL microcentrifuge tube. Bacteria were harvested by centrifuging at 11700 g for 3 min. After removal of supernatant, washed with PBS. Then, 1 mL dye solution in saline at appropriate concentration was added into the microcentrifuge tube. After dispersing with vortex, the bacteria were incubated in a shaking incubator at 37 °C for designed time. Finally imaged by ZEISS LSM800.

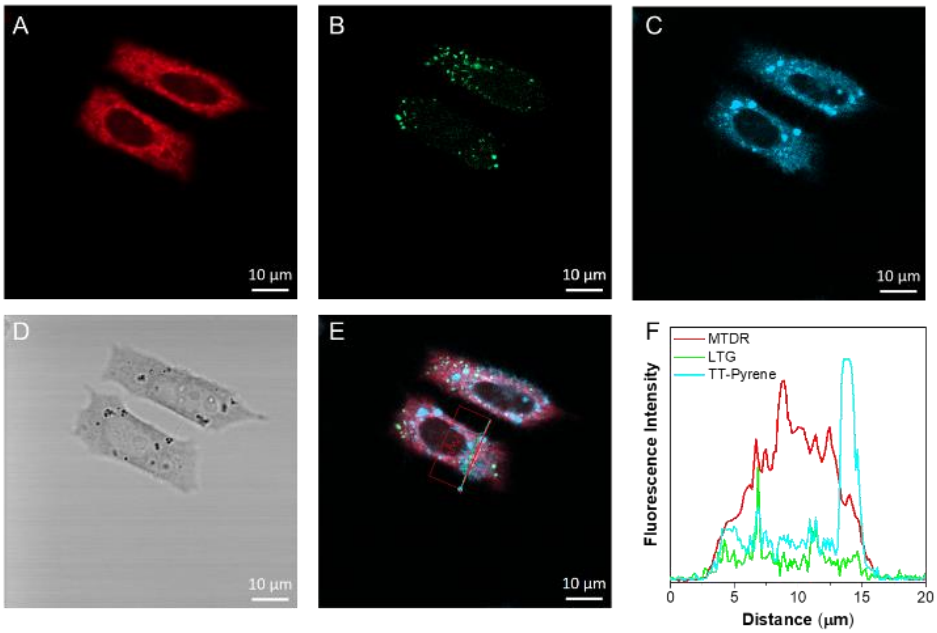

Figure S53. HLF cell co-staining experiment. A) MitoTracker Deep Red. B) LysoTracker Green DND 26. C) **TTPyr** 10 μM. D) Bright field. E) On screen axial fluorescent intensity of **TTPyr**, MitoTracker and LysoTracker. F) Fluorescence intensities of MTDR, LTG, **TTPyr** along the axis.

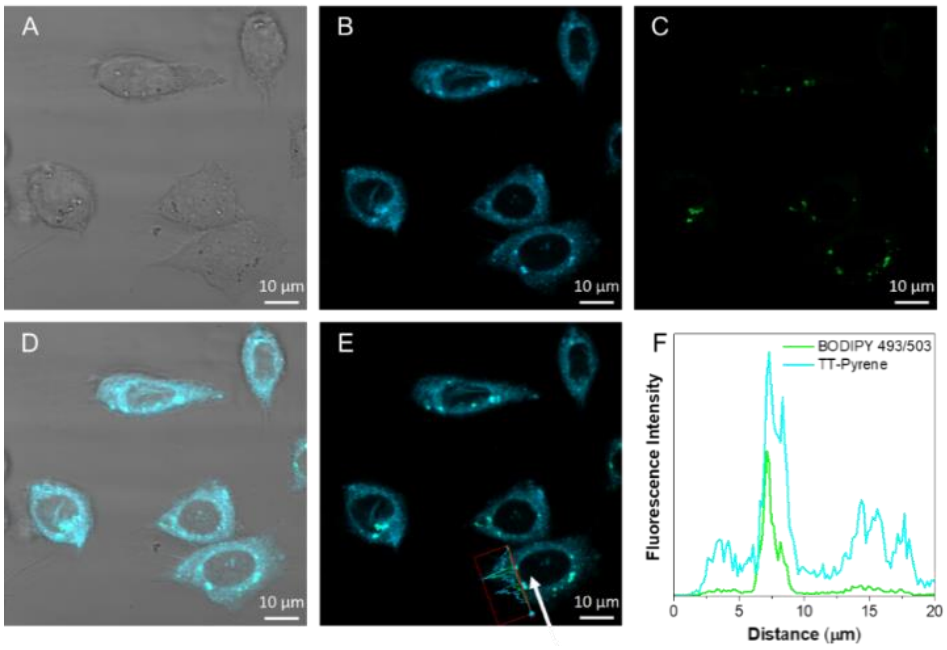

Figure S54. HLF cell co-staining experiment. A) Bright field. B) **TTPyr** 10 μM. C) BODIPY 493/503. D) Merged image of A-C. E) On screen axial fluorescent intensity of **TTPyr** and BODIPY 493/503. F) The fluorescence intensities of **TTPyr** and BODIPY 493/503 along the axis.

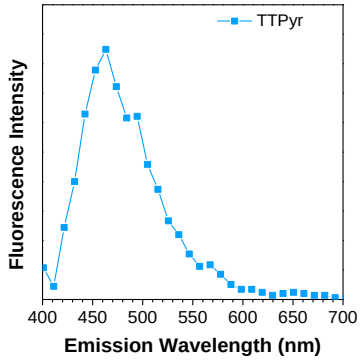

Figure S55. In-situ emission spectra of 10 μM **TTPyr** in HeLa cells obtained on CLSM. λ_{exc} = 405 nm.

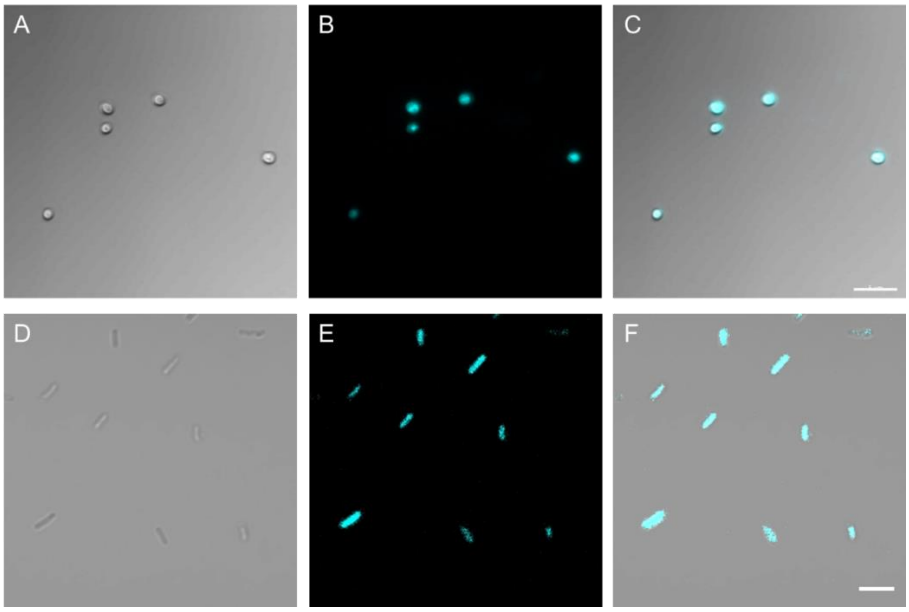

Figure S56. Confocal Laser Scanning Microscope (CLSM) images of bacteria stained with 100 μM **TTPyr** for 60 min. (A-C) *S. aureus*. (D-F) *E. coli*. Scale bar: 5 μm.

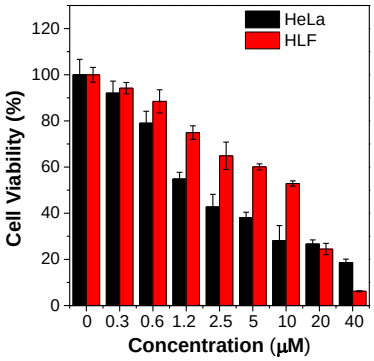

Figure S57. Cell viability of HeLa cells and HLF cells treated with different concentrations of **TTPyr**.

Table S6. Excitation energies (nm), oscillator strength (*f*) and composition of the first singlet transitions and the optimized S_1 transition (S_{1opt}) computed for **TT-Pyr** monomer in HT and RT conformations.[a]

conformation	S_1, *f* weights	S_2, *f* weights	S_3, *f* weights	S_4, *f* weights	S_{1opt}, *f* , τ_{opt} weights
$S_{0,HT}$ (τ_{opt} = 67.4°)	304, *0.229* H-1→L (21%) H-1→L+1 (3%) H→L (**42**%) H→L+1 (26%)	302, *0.257* H-3→L (2%) H-2→L (3%) H-1→L (17%) H-1→L+1 (5%) H→L (**47**%) H→L+1 (22%)	249, *0.004* H-5→L (13%) H→L+3 (3%) H→L+4 (5%) H→L+9 (**64**%)	237, *0.718* H-3→L+5 (2%) H-2→L+4 (2%) H-1→L (**43**%) H→L+1 (**35**%)	370, *0.698* , 41.5° H-1→L+1 (3%) H→L (**94**%)
$S_{0,RT}$ (τ_{opt} = 110.3°)	304, *0.060* H-3→L (4%) H-1→L (**35**%) H→L (10%) H→L+1 (**43**%)	302, *0.498* H-1→L (4%) H-1→L+1 (7%) H→L (**79**%) H→L+1 (5%)	251, *0.008* H-6→L+1 (2%) H-5→L (9%) H→L+3 (7%) H→L+4 (3%) H→L+7 (2%) H→L+9 (**66**%)	238, *0.570* H-2→L+5 (4%) H-1→L (**42**%) H-1→L+1 (2%) H→L+1 (**31**%) H→L+9 (2%)	384, *0.889* , 138.5° H-1→L+1 (3%) H→L (**94**%)

[a]H and L stand for HOMO and LUMO, respectively.

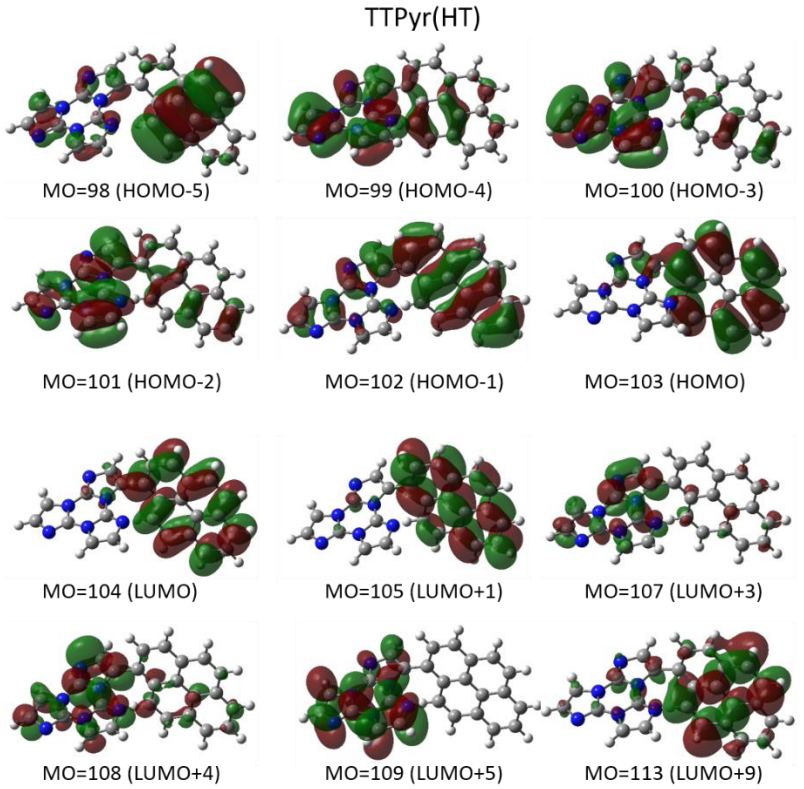

Figure S56. Plots of the ωB97X/6-311++G(d,p) MOs mainly involved in the lowest energy transitions of **TT-Pyr** monomer in HT conformation (isosurfaces value 0.02).

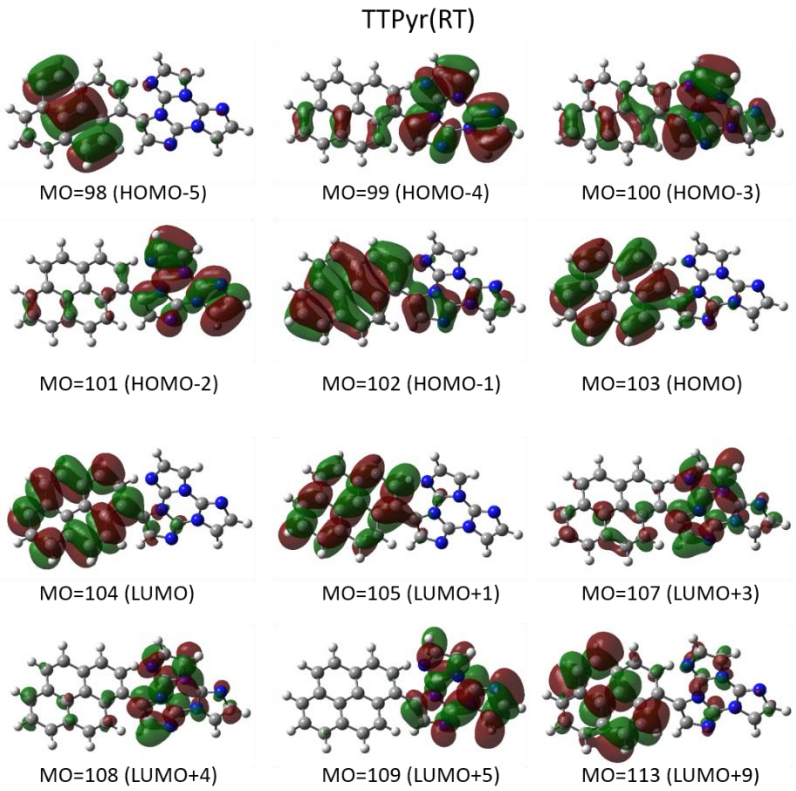

Figure S57. Plots of the ωB97X/6-311++G(d,p) MOs mainly involved in the lowest energy transitions of **TT-Pyr** monomer in RT conformation (isosurfaces value 0.02).

References

[1] D. M. Schubert, D. T. Natan, D. C.Wilson, K. I. Hardcastle, *Cryst. Growth Des.* **2011**, *11*, 843−850.

[2] E. Lucenti, A. Forni, C. Botta, L. Carlucci, C. Giannini, D. Marinotto, A. Pavanello, A. Previtali, S. Righetto, E. Cariati, *Angew. Chem. Int. Ed.* **2017**, *56*, 16302-16307.

[3] K. Suzuki, A. Kobayashi, S. Kaneko, K. Takehira, T. Yoshihara, H. Ishida, Y. Shiina, S. Oishic, S. Tobita, Phys. *Chem. Chem. Phys.*, **2009**, 11, 9850–9860.

[4] Kurtz, S. K., Perry, T. T. (1968). J. Appl. Phys. 39, 3798-3813.

[5] SADABS 2012. Area detector absorption correction. Bruker AXS Inc., Madison, Wisconsin, USA.

[6] M.C. Burla, R. Caliandro, B. Carrozzini, G. L. Cascarano, C. Cuocci, C. Giacovazzo, M. Mallamo, A. Mazzone and G. Polidori "Crystal structure determination and refinement via SIR2014" *J. Appl. Cryst.* **2015**, *48*, 306–309.

[7] G. M. Sheldrick "Crystal Structure Refinement with SHELXL" *Acta Crystallogr., Sect. C: Struct. Chem.* **2015**, *71*, 3–8.

[8] Gaussian 16, Revision A.03, M. J. Frisch, G. W. Trucks, H. B. Schlegel, G. E. Scuseria, M. A. Robb, J. R. Cheeseman, G. Scalmani, V. Barone, G. A. Petersson, H. Nakatsuji, X. Li, M. Caricato, A. V. Marenich, J. Bloino, B. G. Janesko, R. Gomperts, B. Mennucci, H. P. Hratchian, J. V. Ortiz, A. F. Izmaylov, J. L. Sonnenberg, D. Williams-Young, F. Ding, F. Lipparini, F. Egidi, J. Goings, B. Peng, A. Petrone, T. Henderson, D. Ranasinghe, V. G. Zakrzewski, J. Gao, N. Rega, G. Zheng, W. Liang, M. Hada, M. Ehara, K. Toyota, R. Fukuda, J. Hasegawa, M. Ishida, T. Nakajima, Y. Honda, O. Kitao, H. Nakai, T. Vreven, K. Throssell, J. A. Montgomery, Jr., J. E. Peralta,

F. Ogliaro, M. J. Bearpark, J. J. Heyd, E. N. Brothers, K. N. Kudin, V. N. Staroverov, T. A. Keith, R. Kobayashi, J. Normand, K. Raghavachari, A. P. Rendell, J. C. Burant, S. S. Iyengar, J. Tomasi, M. Cossi, J. M. Millam, M. Klene, C. Adamo, R. Cammi, J. W. Ochterski, R. L. Martin, K. Morokuma, O. Farkas, J. B. Foresman and D. J. Fox, Gaussian, Inc., Wallingford CT, 2016.

[9] J.-D. Chai and M. Head-Gordon, *J. Chem. Phys.*, 2008, **128**, 084106.